A 3D bioengineered neural tissue model generated from patient-derived iPSCs develops Alzheimer‘s disease-related phenotypes.

Selene Lomoio[1], Ravi S. Pandey[2], Nicolas Rouleau[3], Beatrice Menicacci[1], WonHee Kim[1], William L. Cantley[3], Philip G. Haydon[1], David A. Bennett[4], Tracy L. Young-Pearse[5], Gregory W. Carter[2,6], David L. Kaplan[3], and Giuseppina Tesco[1#]

Affiliations

[1] Department of Neuroscience, Tufts University School of Medicine, Boston, MA, USA

[2] The Jackson Laboratory for Genomic Medicine, Farmington, CT, USA

[3] Department of Biomedical Engineering, Tufts University, Medford, MA, USA

[4] Rush Alzheimer's Disease Center, Rush University Medical Center, Chicago, IL, USA

[5] Ann Romney Center for Neurologic Diseases, Brigham and Women's Hospital and Harvard Medical School, Boston, MA, USA

[6] The Jackson Laboratory, Bar Harbor, ME, USA

[#] Corresponding author: Giuseppina.Tesco@tufts.edu

Abstract

Background

Current models to study Alzheimer's disease (AD) include cell cultures and animal models. Human diseases, however, are often poorly reproduced in animal models. Developing techniques to differentiate human brain cells from induced pluripotent stem cells (iPSCs) provides a novel approach to studying AD. Three-dimensional (3D) cultures to model AD are represented by organoids, neurospheroids, and scaffold-based cultures.

Methods

We developed a 3D bioengineered model of iPSC-derived neural tissue that combines a porous scaffold composed of silk fibroin protein with an intercalated collagen hydrogel to support the growth of neurons and glial cells into complex and functional networks. This biomaterial scaffold, designed to match the mechanical properties of brain tissue, can support 3D neural cultures for an extended time without necrosis, a fundamental requisite for aging studies.

We have optimized our protocol by seeding neural precursor cells (NPCs) into these scaffolds. Having NPCs stocks derived from multiple subjects allows synchronization of their differentiation and minimizes experimental variability.

Cultures were generated from iPSC lines obtained from two subjects carrying the familial AD (FAD) APP London mutation, two well-studied control lines, and an isogenic control. Cultures were analyzed at 2 and 4.5 months.

Results

An elevated Aβ42/40 ratio was detected in FAD cultures at both time points, as previously reported in 2D cultures derived from the same FAD lines. Extracellular Aβ42 deposition and enhanced neuronal excitability were observed in FAD culture at 4.5 months. Notably, neuronal hyperexcitability has been described in AD patients early in the disease. Transcriptomic analysis

revealed deregulation of multiple gene sets in FAD samples. Such alterations were similar to those observed in human AD brains in a large study that performed a co-expression meta-analysis of harmonized data from Accelerating Medicines Partnership for Alzheimer's Disease (AMP-AD) across three independent cohorts.

Conclusions

Our 3D tissue model supports the differentiation of healthy iPSC-derived cultures in a porous silk-collagen composite sponge with an optically clear central region. This design facilitates nutrient delivery to meet the metabolic demand of long-term cultures. These data provide evidence that our bioengineered model from patient-derived FAD iPSCs develops AD-related phenotypes, including AD transcriptomic features. Thus, it can represent a valuable model for studying AD-related pathomechanisms.

Keywords (3-10)

Alzheimer's disease

Human iPSC

iPSC-derived cultures

Human neural cells

Bioengineered model

3D model

72 **Background**

73 Alzheimer's disease (AD) is a progressive neurodegenerative disorder characterized by memory
74 impairments and cognitive deterioration. It is one of the most common forms of neurodegeneration
75 and accounts for approximately 70% of all cases of dementia. The key pathological hallmarks of
76 AD are extracellular senile plaques composed of neurotoxic amyloid-beta (Aβ) peptide and
77 intracellular neurofibrillary tangles (NFT) composed of hyperphosphorylated tau [1]. Clinical
78 studies show that the most critical risk factors for AD are aging and family history of the disease.
79 Approximately 5% of the population over 65 is affected by AD, and its prevalence doubles with
80 every five years of increasing age [2]. Less than 1% of AD cases occur in families where the
81 disease is inherited in a fully penetrant, autosomal dominant manner, with early (< 65) onset.
82 Three early-onset familial AD (FAD) genes have been identified to date: the amyloid precursor
83 protein (APP) gene, the presenilin 1 (PSEN1) gene, and the presenilin 2 (PSEN2) gene. Together,
84 these genes can harbor any of > 400 mutations (https://www.alzforum.org/mutations) that account
85 for roughly 5-10% of autosomal dominant FAD.

86 Current models to study AD include cell cultures and animal models. Human diseases, however,
87 are often poorly reproduced in animal models [3]. A significant limitation of using rodents to model
88 AD is the increasing evidence for marked differences between humans and rodents in glial gene
89 expression, in contrast to the relatively conserved neuronal gene expression across mammals [4-
90 6]. The development in the past decade of techniques to generate human-induced pluripotent
91 stem cells (iPSCs) and differentiate them into different brain cell types, together with advances in
92 genome editing, has provided a novel model to study AD and other neurodegenerative disorders
93 [7, 8]. Neural cultures derived from patients or isogenic mutant iPSCs recapitulate at least some
94 of the phenotypes observed in the AD brain [7-9]. However, conventional two-dimensional (2D)
95 culture systems fail to recapitulate the diversity and maturation of multiple cell types and their
96 interaction under physiological and pathological conditions. For example, removing secreted Aβ

97 with media changes most likely prevents the deposition of amyloid aggregates in 2D cultures [8].
98 To date, three-dimensional (3D) cultures to model AD are represented by organoids,
99 neurospheroids, and scaffold-based 3D cultures (for review, see [8]).
100 We developed a bioengineered model of iPSC-derived neural tissue [10]. This biomaterial scaffold
101 design was adapted from our previous tissue model generated using primary embryonic rodent
102 brain cells [11] and human-induced neural stem cells [12, 13] to match the mechanical properties
103 of native brain tissue. Our silk-collagen-based "donut" scaffolds can support compartmentalized,
104 3D neural-like tissues for over a year without necrosis [14]. More importantly, our cultures develop
105 networks and action potentials (APs) typical of fully mature neurons [10]. The architecture of the
106 scaffolds was optimized to meet the metabolic demand of high-density cultures in terms of free
107 diffusion of nutrients and oxygen, a fundamental requisite for long-term cultures and aging-related
108 studies.
109 To support that our bioengineered tissue model can reproduce AD-related phenotypes, we have
110 generated cultures from iPSC lines obtained from two subjects carrying the FAD mutation APP
111 V717I (also known as London), hFAD-1, and hFAD-2 (Clone A and B) [15]. As controls, we used
112 two well-studied lines, YZ1 and BR24 [9, 15]. Furthermore, we generated the isogenic control of
113 the hFAD-2 Clone B line by correcting the APP V717I mutation to wild type (C-hFAD-2 Clone B).
114 FAD and control cultures were analyzed at two time points (2 and 4.5 months). An elevated
115 Aβ42/40 ratio was detected in FAD cultures at both time points, as previously reported in 2D
116 cultures derived from the same FAD lines [15].
117 Additionally, extracellular Aβ42 deposition and enhanced neuronal excitability were observed in
118 FAD culture at 4.5 months. Remarkably, neuronal hyperexcitability has been described in both
119 FAD and late-onset AD (LOAD) patients at the early stage of the disease [16]. Gene expression
120 analysis was performed to identify the specific target genes which exhibit significantly increased
121 or decreased expression in FAD lines compared to controls at both time points. Multiple gene

122 sets were deregulated in FAD samples at 2 months. The difference was maintained up to 4.5
123 months. Several of the pathways identified are implicated in neurotransmitter release/reuptake
124 and synthesis/storage, neural connectivity, structural stability of the cytoskeleton, axonal and
125 dendrite structure, and vesicle trafficking regulation. Such alterations in gene expression were
126 similar to those observed in human AD brains in a large study that performed a co-expression
127 meta-analysis of harmonized Accelerating Medicines Partnership for Alzheimer's Disease (AMP-
128 AD) data across three independent cohorts [17]. These data provide compelling evidence that our
129 3D cultures reproduce some of the phenotypes observed in AD patients.
130

131 **Results**

132 **A 3D bioengineered silk-collagen neural model**

133 We have previously designed and validated a 3D bioengineered neural model that combines a
134 porous scaffold composed of silk fibroin with an intercalated hydrogel to allow neurons and glial
135 cells to grow into complex and functional networks [11, 13, 18]. Each element of this model was
136 designed to be tunable, from the pore sizes in the scaffold biomaterial [19] to the hydrogel
137 composition, mechanical properties, and incorporated cell types [14]. We demonstrated that
138 iPSCs incorporated into the scaffolds could directly differentiate into neurons and glial cells and
139 remain functionally active for several months [10].
140 We have optimized our protocol for this study by seeding neural precursor cells (NPCs) instead
141 of iPSCs. This improved protocol offers several advantages: NPCs can be expanded, frozen,
142 banked, and subsequently differentiated. Having NPC stocks derived from multiple subjects
143 allows synchronization of their differentiation and minimizes experimental variability. We have
144 successfully generated NPCs from various iPSC lines using an embryoid body (EB)-based
145 protocol [15, 20-22] that seeks to recapitulate embryonic differentiation. In the absence of
146 exogenous patterning factors, the default path of this protocol is to generate forebrain neurons of
147 cortical fates [23].

148 For the success of this experimental strategy, quality control parameters are associated with iPSC
149 cultures [24]. iPSCs are susceptible to cell culture stresses and prone to genomic instability.
150 Morphology is an obvious indicator of the iPSC health [24]. In our practice, karyotyping, potency,
151 and mycoplasma testing have been routinely performed in all iPSC lines used for this study (Fig.
152 1A-B, Fig. S1).
153 Figure 1C illustrates the timeline schematic for the protocol, in which well-defined and compact
154 iPSC colonies expressing pluripotency markers like the octamer-binding transcription factor 4
155 (Oct4) are differentiated to NPCs over approximately 20 days. The milestones of this approach
156 are the formation of EBs, three-dimensional cell aggregates that mimic some structures of the
157 developing embryo. They can differentiate into all three germ layers [25], followed by neural
158 rosette maturation that can be identified morphologically by their characteristic appearance as
159 round clusters of primitive neuroepithelial cells with apicobasal polarity [26] (Fig. 1C).
160 According to previous work, nestin-positive NPCs can be robustly passaged, frozen, thawed, and
161 differentiated into functional neurons. NPCs could be typically passaged more than ten times in
162 vitro without accumulating karyotype abnormalities [26]; however, in agreement with other studies
163 [26, 27], we found that beyond ten passages, NPCs show increased cellular heterogeneity and
164 lower differentiation efficiency. Thus, experiments were conducted on mycoplasma-free passage-
165 matched NPC populations between passages two and six.
166 When differentiated in 2D on a poly-ornithine/laminin substrate using BrainPhys media
167 supplemented with SM1 and N2, NPCs can efficiently differentiate into human neurons
168 (hNeurons) expressing characteristic markers of a mature neuronal population such as the
169 microtubule-associated protein 2B (MAP2B), the neuron-specific class III beta-tubulin (Tuj1), and
170 synaptophysin (SYN) for extended periods. Glial fibrillary acidic protein (GFAP)-positive cells are
171 also observed, indicating the presence of astrocytic-like cells (Fig. 1D). NPCs have already been
172 described as having dual lineage potential and can differentiate into 70-80% neural populations
173 Tuj1-positive neurons and 20-30% GFAP-positive astrocytes [26].

174 For this study, NPCs have been seeded into silk scaffolds and cultured according to the timeline
175 in Fig. 1E. Our data indicate that NPCs integrate into the silk-collagen scaffold model, expand
176 (NeuroFluor NeuO live staining, Fig. 1E), and differentiate into healthy neurons and astrocytic-
177 like cells, as indicated by IF imaging (Fig. 1F). Cultures express neuronal markers such as
178 neurofilament heavy chain (NFH), MAP2B, and Tuj1 together with GFAP (Fig. 1F). They develop
179 an intricated three-dimensional network extending deep into the silk pores and the supporting
180 collagen, suggesting high connectivity among growing cells (Fig. 1E, F). Cultures generated with
181 this approach supported by BrainPhys media supplemented with SM1 and N2 can survive in
182 culture for extended periods.
183
184 **Aβ42/40 ratio and extracellular Aβ42 deposition are elevated in FAD cultures.**
185 To explore whether our bioengineered cultures could be valuable for modeling AD, we generated
186 cultures from extensively characterized iPSC lines [15] from a father (hFAD-1) and a daughter
187 (hFAD-2), each harboring the FAD mutation APP V717I [15] (Fig. 2A). The father was 57 years
188 old and diagnosed with AD before the biopsy, while the daughter was asymptomatic at age 33.
189 The two clones from the daughter (hFAD-2 Clone A and Clone B) displayed a normal euploid
190 karyotype (Fig. S1), while the clone from the father (hFAD-1) revealed a standard chromosome
191 number but a balanced (t(1;12)(q42.3;q21.2)) translocation in all cells analyzed (Fig. S1). The
192 fibroblasts obtained from this subject displayed the same abnormal karyotype, suggesting a
193 preexisting abnormality that did not arise during the reprogramming [15]. This karyotypic alteration
194 didn't compromise the differentiation potential for the line.
195 The following lines were selected as controls (Fig. 2A). YZ1 [15], derived from fetal lung
196 fibroblasts, BR24 (Religious Order Study (ROS) or Rush Memory and Aging Project (MAP) [28]),
197 a cognitively unimpaired woman at the time of biopsy, 76 years of age [9]. Participants in the ROS
198 and MAP projects range from 50 to over 100 years and are free of dementia at the enrollment [9,
199 28]. Follow-up assessments indicated that the BR24 subject died at the age of 90, showing no

200 signs of cognitive decline or AD pathology. We also generated an isogenic control for the hFAD-
201 2 Clone B line (Fig. 2B) using genome-editing technology by reverting the APP V717I mutation to
202 wild type (C-hFAD-2 Clone B). Potential off-target cuts were identified using the Cas-OFF finder
203 (http://www.rgenome.net/cas-offinder). The top 8 sites were amplified, and Sanger sequenced to
204 verify the status of these potential off-targets. None of the predicted sites showed evidence of off-
205 targeting cutting. No karyotype clonal abnormalities were identified among the control lines (Fig.
206 S1).
207 To better understand the nature of our cultures and the reproducibility of the differentiation
208 approach from different iPSC lines and clones, we next turned to NanoString Technologies® for
209 measuring gene expression at 2 and 4.5 months. Data were analyzed by ROSALIND®
210 (https://rosalind.onramp.bio), with a HyperScale architecture developed by ROSALIND®, Inc.
211 (San Diego, CA, USA) and the nCounter® Advanced Analysis protocol. Housekeeping probes (9)
212 used for normalization were selected based on the geNorm algorithm implemented in the
213 NormqPCR R library.
214 We used the nCounter® Cell Type Profiling Module (as described in [29]) to assess the abundance
215 of various cell populations (Fig. 2C). The method quantifies cell populations using marker genes
216 expressed stably and precisely in given cell types. While markers for endothelial cells,
217 oligodendrocytes, astrocytes, neurons, and microglia have been screened, only scores for
218 neurons and astrocytes reached a statistically significant threshold (p-value <0.001 and <0.01,
219 respectively, Fig. 2C), indicating that these two cell types are the main constituents of our cultures.
220 Exploiting NanoString normalized expression analysis, we compared the expression of specific
221 groups of commonly expressed genes in iPSC-derived neural cultures (Fig. S2) based on
222 previous studies [15, 20, 23, 30-32] between different lines, genotypes, time points, and biological
223 replicates. In agreement with previous observations [15, 20], normalized expression analysis
224 identified the enrichment of a vast array of glial (GFAP, ALDH1L1, S100B, etc.), pan-neuronal
225 and synaptic markers (HOMER1, TBR1, STX1A, etc.) with most neurons exhibiting an excitatory

226 profile, together with some progenitor markers (NES, CCND1) being expressed up to 4.5 months
227 post-seeding. As expected, based on the differentiation method implemented, genomic analysis
228 suggests that our culture acquired a cortical layer fate as indicated by the expression of genes
229 (TBR1, DLX1, DLX2, etc.) involved in mammalian neocortical development and/or expressed in
230 a layer-specific manner in the human neocortex (Fig. S2) [33]. Also, AD-related genes were
231 expressed in our 3D cultures across all analyzed conditions. Differential expression analysis did
232 not reveal any significant variance between lines and genotypes for this set of genes, suggesting
233 that the cultures are homogeneously patterned and that the differentiation approach is highly
234 reproducible.
235 To assess whether our cultures can recapitulate some AD-related phenotypes, soluble Aβ
236 quantification (MSD: Meso Scale Discovery Assay, Aβ Peptide Panel 1-4G8) was performed on
237 24-hour-conditioned media (Fig. 2D). In agreement with previous reports [15, 23, 34, 35], the
238 Aβ42 over Aβ40 ratio was found to be increased in FAD cultures compared to control ones at
239 both time points (CTR 2mo: 0.040±0.002 vs. FAD 2mo: 0.089±0.017, p=0.0003; CTR 4.5mo:
240 0.048±0.004 vs. FAD 4.5mo: 0.093±0.005, p<0.0001). The Aβ42/40 ratio calculated for the
241 isogenic C-hFAD-2 Clone B control was comparable to that of other control lines, supporting the
242 idea that the observed increase in the hFAD-2 Clone B depended on the APP V717I mutation.
243 Next, we performed IF using an antibody specific for Aβ42 (validated in 5XFAD:BACE1$^{-/-}$ brain
244 sections [36]) and calculated the amyloid burden for CTR and FAD cultures at both time points
245 (Fig. 2E). Confocal imaging and 3D reconstruction revealed the presence of Aβ42-positive
246 extracellular aggregates interspersed among FAD hNeurons (identified by MAP2B staining, Fig.
247 2F). Volumetric analysis of the amyloid burden (Fig. 2E) revealed a mild trend for increase starting
248 at 2 months in FAD cultures compared to controls (CTR: 0.00053±0.00022 vs. FAD:
249 0.00170±0.00044, p=0.9368) with a striking difference among conditions at 4.5 months (CTR:

250 0.00028±0.00005 vs. FAD: 0.02572±0.00281, p<0.0001). No difference was identified between
251 control groups at the two time points analyzed.
252
253 **FAD cultures manifest enhanced neuronal excitability**
254 To determine the electrophysiological properties of the cultures, local field potentials (LFPs) were
255 recorded from single electrodes inserted into the superficial layers of the hydrogel next to silk
256 fibers, adapting a protocol by Du and collaborators [37], where both spontaneous and evoked
257 potentials (EPs) were collected. LFPs, indicative of cellular electrical activations [14], were
258 quantified and compared across all conditions. The spontaneous and evoked activity was
259 observed within all the scaffolds analyzed starting at 2 months, suggesting that our 3D model is
260 populated by functional neurons capable of network activity.
261 Evidence indicates that LOAD and FAD patients show enhanced excitability, with onset during
262 the early stages of the pathology [38-45]. In our study, FAD cultures displayed comparable levels
263 of spontaneous potentials (Log10 LFP spikes/min) relative to control samples at 2 months (CTR:
264 0.717±0.130 vs. FAD: 0.872±0.126, p=0.3950); however, by 4.5 months, FAD samples displayed
265 significantly more spontaneous potentials relative to controls (CTR: 0.515±0.106 vs. FAD:
266 0.832±0.114, p=0.0475). Similarly, FAD samples showed more EPs relative to controls at 4.5
267 months post-seeding (CTR: 0.736±0.079 vs. FAD: 1.050±0.077, p=0.0064), which was not
268 apparent at 2 months (CTR: 1.040±0.091 vs. FAD: 1.270±0.112, p=0.1069). Our findings agree
269 with previous work that indicates dysregulation of the electrophysiological properties in AD brains
270 accompanied by enhanced network activity. Cognitive impairment in AD patients was assumed
271 to originate from depressed synaptic activity that eventually led to neurodegeneration. However,
272 multiple lines of evidence now indicate that, particularly during AD initial stages, synapse
273 dysfunctions are first induced by neuronal hyperactivity rather than hypoactivity [46-48].
274
275

276 **Differential expression and functional analysis of the NanoString panel in FAD cultures**

277 Transcriptional profiling of NanoString data from our samples was performed by ROSALIND®
278 platform (see method section for details). At 2 months, there were 133 differentially expressed
279 genes (DEGs) (absolute fold change > 1.5 & FDR < 0.05) between FAD and control samples (Fig.
280 4A). Expression for 38 of those 133 genes was upregulated in FAD samples compared to controls
281 and downregulated for 95 of 133 genes (Fig. 4A). Gene set analysis (GSA) identified increased
282 expression of genes associated with Cytokines, Activated Microglia, and Neuronal Cytoskeleton
283 (directed GSS > 0) (Fig. 4C).

284 Based on the differentiation protocol used for this study, we expected our cultures to be populated
285 exclusively by cells derived from the neuroectodermal lineage. So, we were surprised to observe
286 an upregulation of the Activated Microglia pathway in FAD cultures. Follow-up
287 immunofluorescence for TMEM119 (Fig. S3), a well-known microglia marker, followed by confocal
288 microscopy identified the presence of TMEM119 positive cells in the scaffolds interspersed
289 among MAP2 and GFAP-positive cells, indicating the presence of microglia-like cells in our
290 cultures. The cells show a ramified morphology and are intertwined with neuronal processes as
291 described by others (Fig. S3) [49]. These data agree with previous studies that have identified
292 mesoderm-derived progenitors and microglia in cerebral organoids [49, 50].

293 Further, GSA identified reduced expression of genes associated with multiple other
294 neurodegeneration pathways such as Transmitter Release, Neural Connectivity, and Vesicle
295 Trafficking (directed GSS < 0) (Fig. 4C).

296 At 4.5 months, there were 38 DEGs (absolute fold change > 1.5 & p < 0.05) between FAD and
297 control samples (Fig. 4B). Expression for 5 of the 38 genes was upregulated in FAD samples
298 compared to controls and downregulated for 33 of 38 genes (Fig. 4B). Gene set analysis identified
299 increased expression of genes associated with Cytokines and reduced expression of genes
300 associated with multiple pathways such as Transmitter Release, Neuronal Cytoskeleton, and
301 Vesicle Trafficking (Fig. 4D).

302 **FAD cultures reproduce human neurodegeneration signatures**

303 To assess the relevance of our model for AD, we performed a correlation analysis between our
304 NanoString data from FAD cultures and human post-mortem co-expression modules [17, 51].
305 FAD cultures at 2 months showed significant positive correlations ($p<0.05$) with AD-associated
306 changes in human co-expression modules in Consensus Cluster B, which include transcripts that
307 are enriched for immune-related pathways in the cerebellum brain region (CBEturquoise) (Fig.
308 5A). Furthermore, FAD cultures at 2 months showed significant positive correlations ($p<0.05$) with
309 AD changes in multiple modules in Consensus Cluster C, which include transcripts that are
310 enriched for neuronal-related pathways in the inferior frontal gyrus module (IFG), temporal cortex
311 (TCX), and the parahippocampus gyrus (PHG) brain regions (Fig. 5A). However, these significant
312 positive correlations diminish at 4.5 months (Fig. 5A). Interestingly, FAD cultures at 2 months
313 showed a significant positive correlation (Pearson Correlation = 0.27; $p<0.05$) with AD ECM
314 organization changes in module TCXblue in Consensus Cluster A but also showed a significant
315 negative correlation (Pearson Correlation = -0.35; $p<0.05$) with AD changes in the PHGyellow
316 module enriched for similar biological process. However, at 4.5 months of age, FAD cultures
317 exhibited a non-significant but positive correlation with AD changes in the PHGyellow module
318 (Pearson Correlation = 0.11; $p > 0.05$) and a stronger significant positive correlation with TCXblue
319 module changes in AD (Pearson Correlation = 0.27; $p < 0.05$) (Fig. 5A). These results suggest
320 that functional changes such as ECM organizations are strengthened with age and represent
321 similar effects to those observed in endpoint AD.

322 Next, we examined the expression profile of differentially regulated genes in the FAD cultures
323 identified by the ROSALIND® platform across human AMP-AD transcriptomic data. We
324 determined that most of the differentially upregulated genes (fold change > 1.5) in 2-month-old
325 FAD cultures showed increased expression in immune/inflammation-associated AMP-AD
326 modules in Consensus Cluster B (Fig. 5B), suggesting increased expression of these genes in
327 multiple human brain regions. Similarly, most of the differentially downregulated genes (fold

328 change < 1.5) in 2 months old FAD cultures showed reduced expression across numerous human
329 brain regions except in the frontal pole and cerebellum brain regions of AD patients (Fig. 5C). Our
330 2-month-old FAD cultures exhibited expression profiles of neuronal genes remarkably similar to
331 human AD for multiple brain regions.
332 Similarly, we examined the expression of differentially deregulated genes in 4.5 months old FAD
333 cultures across AMP-AD modules. There were only 5 genes that were differentially upregulated
334 in the 4.5-month-old FAD cultures compared to controls, and these genes mainly exhibited
335 reduced expression in some of the AMP-AD modules (Fig. S4 A). Most of the differentially
336 downregulated genes (fold change < 1.5) in 4.5 months old FAD cultures showed reduced
337 expression in neuronal-associated AMP-AD modules in Consensus Cluster C, except in
338 CBEyellow and FPyellow modules (Fig. S4 B). These results suggest that neurodegeneration-
339 related genes were downregulated in our FAD cultures, similar to human AD patients.
340
341 **Discussion**
342 We report here that iPSC-derived NPCs reliably integrate into the silk-collagen scaffold model,
343 expand, and differentiate in healthy neurons and astrocytic-like cells as indicated by the
344 expression of neuronal and astrocytic markers. Accordingly, gene expression and cell enrichment
345 analysis revealed a similar cellular composition across all cultures. More importantly, 3D neural
346 cultures from APP London mutation heterozygous carriers recapitulate some AD-like phenotypes.
347 We found that FAD cultures displayed an elevated Aβ42/40 ratio in conditioned media at 2 and
348 4.5 months, as previously reported in 2D cultures derived from the same FAD lines [15, 23]. While
349 the Aβ42/40 ratio change was similar at the two time points, extracellular deposition of Aβ42
350 developed only in the older cultures and identified FAD from control cultures. Notably, Aβ42/40
351 ratio and Aβ42 extracellular deposition in the isogenic control cultures were similar to BR24 and
352 YZ1 lines. These data demonstrate that the APP V7171I mutation causes such phenotypes.

353 LFP recordings showed that our 3D cultures were electrically active starting at 2 months. While
354 no difference in LFP frequency was observed at 2 months, by 4.5 months, FAD samples displayed
355 significantly higher spontaneous and evoked potentials relative to controls. The increased
356 excitability in FAD cultures correlated with extracellular Aβ42 deposition but not with soluble
357 Aβ42/40 ratio levels, as they were similar at both time points. These data suggest that extracellular
358 Aβ deposition may trigger enhanced network activity. Our data agree with previous work showing
359 increased neuronal excitability in AD patients at an early stage of the disease [16, 43].
360 A large study conducted on carriers of FAD mutations (The Dominantly Inherited Alzheimer
361 Network (DIAN) consortium) showed that changes in cerebrospinal fluid (CSF) biomarkers,
362 cerebral amyloid deposition, and brain metabolism begin at least two decades before the
363 predicted onset of clinical symptom [52]. Similarly, increased brain activity may precede AD
364 diagnosis by 30 years in PSEN1 mutation carriers [53, 54]. More recently, neuronal
365 hyperexcitability was described in organoids generated from isogenic iPSC lines carrying the FAD
366 PSEN1 ΔE9, PSEN1 M146V, or APP Swedish mutations [55]. However, this is the first report of
367 enhanced excitability in 3D cultures from patient-derived iPSC lines carrying the APP London
368 mutation.
369 Differential expression analysis and GSA revealed that multiple gene sets were deregulated in
370 FAD compared to control cultures. At 2 months, upregulated genes were associated with
371 Cytokines, Activated Microglia, and Neuronal Cytoskeleton pathways in GSA. The downregulated
372 genes were related to multiple neurodegeneration pathways such as Transmitter Release, Neural
373 Connectivity, and Vesicle Trafficking. Some of the differences were maintained for up to 4.5
374 months. At 4.5 months, GSA identified increased expression of genes associated with Cytokines
375 and reduced expression of genes associated with multiple pathways such as Transmitter
376 Release, Neuronal Cytoskeleton, and Vesicle Trafficking. While most DEGs in the FAD cultures
377 are expressed in neurons, genes associated with activated microglia were upregulated in FAD

378 cultures at 2 months. Even though only scores for neuronal and astrocyte markers reached a
379 statistically significant threshold in the nCounter® Cell Type Profiling Module, TMEM119-positive
380 cells are present in our cultures. Similarly, mesoderm-derived progenitors, from which microglia
381 originate, and mature microglia-like cells innately develop in cerebral organoids [49, 50].
382 To validate our cultures as an AD model in vitro, we applied a system biology approach developed
383 to evaluate AD mouse models [51]. A correlation analysis was performed between gene
384 expression changes in FAD cultures and changes in human AD cases in post-mortem co-
385 expression modules. We used a recent human molecular disease catalog based on harmonized
386 co-expression data from three independent postmortem brain cohorts (ROSMAP, Mayo, Mount
387 Sinai Brain bank) [56-58] and seven brain regions that define 30 human co-expression modules
388 and five consensus clusters derived from the overlap of those modules [17]. FAD cultures at 2
389 months showed significant positive correlations with human co-expression modules in Consensus
390 Cluster B, including transcripts enriched for immune-related pathways. They showed significant
391 positive correlations with multiple modules in Consensus Cluster C, including transcripts enriched
392 for neuronal-related pathways. However, these significant positive correlations diminish at 4.5
393 months of age.
394 Next, we examined the expression profile of differentially regulated genes in the FAD cultures
395 identified by the ROSALIND® platform across human AMP-AD transcriptomic data. We
396 determined that most of the differentially upregulated genes in 2-months-old FAD cultures showed
397 increased expression in immune/inflammation-associated AMP-AD modules in Consensus
398 Cluster B. Similarly, most of the differentially downregulated genes in 2-months-old FAD cultures
399 showed reduced expression across numerous human brain regions in Consensus Cluster C.
400 Thus, 2-month-old FAD cultures exhibited expression profiles of neuronal genes remarkably
401 similar to human AD for multiple brain regions. In the 4.5-month-old FAD cultures, most
402 differentially downregulated genes showed reduced expression in neuronal-associated AMP-AD

403 modules in Consensus Cluster C. These results suggest that neurodegeneration-related genes
404 were downregulated in FAD cultures, similar to human AD patients.
405 Since iPSC reprogramming rejuvenates cells and erases donor aging signatures, concerns were
406 raised about the ability to model age-related diseases with iPSC-derived neuronal cultures [59].
407 It is well-established that AD develops over decades [60]. Thus, genetic factors may produce
408 endophenotypes early in life; therefore, they can be captured in iPSC-derived neural cultures.
409 Altogether these data provide compelling evidence that our iPSC-derived 3D cultures reproduce
410 some of the phenotypes observed in AD patients.
411
412 **Conclusions**
413 We developed a neural tissue model that supports the differentiation of iPSC-derived NPCs in a
414 donut-shaped porous silk sponge with an optically clear (collagen-filled) central region. The
415 porous design facilitates nutrients and oxygen diffusion to meet the metabolic demand of long-
416 term cultures. This study provides compelling evidence that our 3D bioengineered model from
417 patient-derived FAD iPSCs develops AD-related phenotypes, including AD transcriptomic
418 features. Thus, this represents a valuable in vitro model for investigating AD-related
419 pathomechanisms, identifying potential therapeutic targets, and drug screening.
420 As discussed, one of the main strengths of this model is that every element was designed to be
421 tunable and amenable to experimental modification. Although we did not incorporate a layered
422 structure for this study, the 3D model can be designed using a concentric toroidal scaffold to more
423 closely approximate gross features of the layered brain tissue [11]. However, we need to consider
424 that any modification to the structural design of the model could cause unexpected changes to
425 the integrity and longevity of the cultures [14] and therefore require extensive and costly
426 troubleshooting. We could also incorporate embedded electrodes for continuous, long-term
427 recordings of electrophysiological activity [61, 62]. Notably, the model could include controlled co-
428 cultures of neural cells (neurons, astrocytes, and microglia) derived from different donors,

429 selectively mutated or otherwise, or exposed to environmental conditions hypothesized to drive
430 or exacerbate neurodegeneration [14].
431 On the other hand, our model still has technical limitations. Even though the porous structure of
432 the scaffolds facilitates the diffusion of oxygen and nutrients, it lacks a proper neurovascular unit,
433 a perivascular compartment, and coordinated drainage of accumulated metabolites. This could
434 affect, among other things, the optimal and homogenous penetration of drugs and their clearance.
435 In addition, other practical challenges like scalability and high throughput screening compatibility
436 will have to be optimized.
437
438 **Methods**
439 **iPSC lines**
440 hFAD-1, hFAD-2 Clone A and B iPSC lines [15] were generated in the laboratory of Dr. T. Young-
441 Pearse (Brigham and Women's Hospital, Boston, MA, USA). BR24 iPSC line (ROSMAP) [9, 28]
442 was generated at the New York Stem Cell Foundation. YZ1 iPSC line was obtained from the
443 University of Connecticut-Wesleyan Stem Cell Core (Farmington, CT, USA [15]). The original
444 manuscripts cited above describe the reprogramming methods and quality control assays for
445 these lines.
446 hFAD-2 Clone B Corrected was generated at the University of Connecticut-Wesleyan Stem Cell
447 Core (Farmington, CT, USA). Briefly, the guide RNA used for APP editing was designed using
448 chop-chop (https://chopchop.cbu.uib.no/) for specificity to the loci of interest. The resulting guide
449 5' GACAGTGATCATCATCACCT 3' was identified to have high specificity to the desired loci. The
450 guide is designed to cut the mutant allele. Given that the CAS9/guide RNA was transiently
451 expressed in the cells, the potential for off-targets in the nearest matches was minimal. Potential
452 off-targets were identified using the Cas-OFF finder (http://www.rgenome.net/cas-offinder/). The
453 top eight identified sites were amplified from the clones, and Sanger sequenced to verify the
454 status of these potential off-targets. None of the predicted sites showed evidence of off-targeting

455 cutting. After targeting, the corrected allele resulted in a single base difference from the original
456 guide sequence. None of the clones sequenced exhibited off-target cutting at the predicted sites
457 or the corrected allele.
458 All iPSC lines have been confirmed by sequencing before starting any of the experiments listed
459 in this manuscript.
460
461 **ROSMAP study participants**
462 iPSC lines were generated from autopsied participants in either the Religious Orders Study or
463 Rush Memory and Aging Project (ROSMAP) [28]. Both studies were approved by an Institutional
464 Review Board of Rush University Medical Center; they enroll older persons without dementia who
465 agree to annual clinical evaluation and brain donation at death. All participants signed informed
466 consent, an Anatomical Gift Act, and a repository consent to allow their resources to be
467 repurposed. As part of the annual evaluation, peripheral blood mononuclear cells were drawn and
468 cryopreserved.
469
470 **Karyotype analysis and mycoplasma testing**
471 G-banded karyotyping was outsourced to WiCell (Madison, WI, USA). WiCell's chromosome
472 analysis is optimized for pluripotent stem cells. All results are reviewed by an American Board of
473 Medical Genetics and Genomics (ABMGG) board-certified or board-eligible director. Karyograms
474 for all the lines have been checked every ten passages.
475 Mycoplasma testing was performed monthly for all the lines included in this study at any
476 differentiation stage (LookOut Mycoplasma PCR Detection Kit, Sigma). All cells used in this study
477 were consistently negative.
478
479
480

481 **NPC differentiation**

482 iPSCs were maintained in feeder-free conditions on plates coated with Matrigel hESC-qualified
483 Matrix (Corning) with daily media changes using mTeSR1 medium (StemCell Technologies).
484 Cells were held at 37°C and 5% CO_2 and were split as necessary based on colony growth (5-7
485 days). Cells were passaged in small aggregates (1:7/1:10 depending on the line) using ReLeSR
486 (StemCell Technologies). 10 µM Y-27632 (ROCK inhibitor, StemCell Technologies) were added
487 to the culturing media for a maximum of 24 hours after passage.

488 According to the StemCell Technologies method, NPCs were differentiated using an EB-based
489 protocol without SMADi supported by STEMdiff Neural Induction medium (StemCell
490 Technologies) with daily media change over ~20 days. To generate iPSC-derived EBs for neural
491 induction AggreWell 800 (StemCell Technologies), 24-well plates were used. These plates enable
492 the easy generation of uniformly sized EBs, making differentiation experiments more
493 reproducible. For each well of the AggreWell plate, $3x10^6$ single-cell suspension (Gentle Cell
494 Dissociation Reagent, StemCell Technologies) of iPSCs were plated, followed by centrifugation
495 at 100xg for 3 minutes, to capture the cells in the microwells. A daily partial-medium change was
496 performed for 4 days. On day 5, EBs were harvested from a single well of an AggreWell 24-well
497 plate and re-plated onto a Matrigel hESC-qualified-coated well of a tissue culture-treated 6-well
498 plate. Replated EBs were maintained with daily media change until neural rosette structures were
499 visible and defined. Around days 10-12, based on the different lines, rosettes were selected
500 (Neural Rosette Selection Reagent, StemCell Technologies) and replated onto Matrigel hESC-
501 qualified Matrix-coated plates. Selected rosette-containing clusters attach, and NPC outgrowths
502 will form a monolayer between the clusters. A daily full-medium change was performed. NPCs
503 are ready for passage 1 at approximately day 17-19 (Accutase, StemCell Technologies). NPCs
504 were plated at $1.25x10^5$ cells/cm^2 on Matrigel hESC-qualified Matrix-coated wells and maintained
505 in Neural Progenitor medium (StemCell Technologies) with daily complete media change. Single-
506 cell suspensions ($2x10^6$ cells/mL) of NPCs were cryopreserved and banked for future usage using

507 Neural Progenitor Freezing (StemCell Technologies). At least two separate differentiations of
508 NPCs have been generated from different iPSC stocks for all the lines included in this study and
509 used to differentiate hNeurons.
510
511 **Scaffold preparation, seeding, and differentiation into hNeurons**
512 Silk protein was processed from *Bombyx mori* cocoons as described previously [63]. In brief, silk
513 cocoons were cut into fragments and boiled for 30 minutes in a 0.02 M Na_2CO_3 solution. The
514 fibroin was solubilized in a 9.3 M LiBr solution dialyzed against deionized water. The silk solution
515 was then diluted to 6% weight/volume and used to generate the porous scaffolds via salt leaching
516 [19], using 500–600 um NaCl crystals to generate a sponge-like structure. A biopsy punch was
517 used to generate the donut-shaped scaffolds (5mm outer diam. x 2mm central hole diam. x 2mm
518 ht.). Scaffolds were autoclaved and then coated with poly-L-ornithine (20ug/mL in DPBS, Sigma)
519 and laminin (10ug/mL in DMEM/F-12, Sigma) overnight at 4°C.
520 A strained (40um nylon mesh) single-cell suspension of ($2x10^6$/100 uL) NPCs between passages
521 two and six was added to the coated scaffold in a 96-well plate and incubated for 24 hours. The
522 media (200uL, Neural Progenitor medium) was changed daily for five days following seeding,
523 moving the scaffolds to fresh wells with each change. After allowing five days of cellular
524 expansion, the scaffolds were moved to a clean well and infused with a 100 uL solution of cold
525 Collagen Type-1 Rat Tail (3.0mg/mL, Corning) mixed with 10X PBS and 1N NaOH (ratio 88:10:2).
526 The collagen-filled scaffolds were then incubated at 37°C until the gelation occurred (~45
527 minutes). Once solidified, the scaffolds were transferred to a 24-well plate and flooded with 1.5
528 mL of BrainPhys media (StemCell Technologies) supplemented with SM1 (StemCell
529 Technologies) and N2 (ThermoFisher) with media changes every four days and differentiated into
530 hNeurons.
531
532

533 **Immunofluorescence and imaging analysis**

534 2D and 3D cultures were fixed with a 4% paraformaldehyde/4% sucrose solution in DPBS for 15
535 and 30 minutes, respectively, followed by membrane permeabilization with 0.3% Triton X-100 for
536 15 minutes. Non-specific binding sites were blocked for one (2D) or four (3D) hours at RT (5%
537 BSA, 0.1% Triton-X-100 in DPBS). Cultures were then incubated with primary antibodies (see
538 Antibody Table) diluted in 1% BSA, 0.1% Triton-X-100 in DPBS overnight at 4°C. After multiple
539 washes in DPBS, sections were incubated with Alexa (1:1000 in 1% BSA in DPBS) fluorescent
540 secondary antibodies against the corresponding host species for one (2D) or three (3D) hours at
541 RT. Nuclei were stained with DAPI (Sigma). 2D cultures were mounted on superfrost slides
542 (Fisher Scientific) using Fluoromount-G1 mounting media (Southern Biotech), while 3D cultures
543 were imaged directly.

544 NeuroFluor™ NeuO (StemCell Technologies), a membrane-permeable fluorescent probe that
545 selectively labels iPSC-derived neurons, was used to stain live cultures according to manufacture
546 instructions.

547 Z-stack fluorescence images were obtained using confocal microscopes (SP8 Falcon Leica, SP8
548 Leica, see figure legends for details), keeping constant imaging parameters. 3D reconstructions
549 were generated with the LAS X Life Science Leica software. Image analysis was performed using
550 Fiji ImageJ version: 2.0.0-rc-69/1.52p.

551 Aβ burden volumetric analysis was performed using the Fiji ImageJ plug-in 3D object counter.
552 The sum of all extracellular Aβ deposition volumes was divided by the total volume of the region
553 of interest (ROI) imaged to obtain the amyloid burden values. At least two separate sets of cultures
554 per line and three images per set of cultures have been analyzed.

555

556 **MSD assay and data analysis**

557 Before harvest, BrainPhys media was changed, and fresh media was dispensed into each well.
558 Twenty-four hours later, media was collected and stored at -80°C. MSD (Rockville, MD, USA)

559 assay for the detection of human Aβ38, Aβ40, and Aβ42 (V-PLEX Aβ Peptide Panel 1 (4G8) Kit)
560 was performed in-house according to the manufacturer's instructions on undiluted conditioned
561 media. Technical duplicates were run for all the samples analyzed. The assay demonstrated high
562 sensitivity with a lower limit of detection values in the low-pg/mL and over 2.5 logs of dynamic
563 range, allowing the measurement of analytes in all samples, except for Aβ38, which fell under the
564 lower limit of detection for most of the samples. All MSD assays exhibited excellent reproducibility
565 with an average calculated concentration of 3.6% and 7.2% for the standards and samples within
566 the detection range of the assay, respectively. The data were analyzed using MSD Workbench
567 4.0 software. The software fits the standard curves using a four-parameter logistic fit with $1/y^2$
568 weighting.
569
570 **LFP recordings**
571 Local field potentials (LFPs) were recorded from samples, adapting a protocol by Du et al. [37].
572 Both spontaneous and evoked potentials (EPs) were collected. Each sample was placed in the
573 center of a 35mm plastic petri dish (Corning) containing 2 mL of an extracellular solution
574 simulating cerebrospinal fluid (mM): 130 NaCl, 1.25 NaH_2PO_4, 1.8 $MgSO_4$, 1.6 $CaCl_2$, 3 KCl, 10
575 HEPES-NaOH, 5.5 glucose, pH 7.4. The dish and solution were maintained at 37ºC using a WP-
576 16 Warmed Platform (with a TC-134A Handheld Temperature Controller). A bipolar stimulator
577 was positioned on top of the sample, affixing it to the bottom of the dish. Then, a recording
578 electrode (borosilicate glass pipette, 40-80 MΩ resistance) which was pulled with a Sutter P-97
579 (Navato), was inserted into the silk-scaffold region between the stimulators (e.g., stimulator-
580 electrode-stimulator). LFPs were amplified and digitized (Axon Instruments DAC; Intan digital
581 amplifier) with a sampling frequency of 2500Hz. Recordings were performed blind (each sample
582 was given an unidentifiable ID), always counterbalanced by condition, and replicated batches
583 were measured within the same 12-hour window.

584 Spontaneous activity (baseline) was recorded for 2 mins, followed by the evoked potential phase,
585 which consisted of a 60s period of stimulation (1ms pulse, 1Hz, 5 mA), an injection of 10 μM
586 tetrodotoxin (sodium channel blocker), 2 mins of perfusion, and a final 60 sec period of stimulation.
587 Data were retrieved from Clampex 10.7 (Axon Instruments), exported to Clampfit 10.7, and
588 "spikes" indicative of activity were extracted using an amplitude threshold (±0.35 mV). Spike
589 frequencies (LFP spikes/minute) were computed for spontaneous (baseline) recordings. Evoked
590 potentials per stimulation period were also quantified after a background-subtraction process as
591 previously described [37]. All data were normalized to DNA content quantified using Quant-iT
592 PicoGreen dsDNA Assay kit (ThermoFisher). Data were also subjected to a log-10 transformation
593 to stabilize and normalize expected trial-to-trial variation.
594
595 **RNA isolation and NanoString outsourcing**
596 At the time of desired analysis, scaffolds were snap-frozen using liquid nitrogen and stored at
597 −80°C. The frozen scaffolds were then homogenized using a liquid nitrogen-chilled Spectrum
598 Bessman Tissue Pulverizer (Fisher Scientific). RNA from homogenized samples was extracted
599 immediately after the homogenization using the RNeasy Plus Mini kit (Qiagen) following the
600 manufacturer's instructions. Briefly, samples were dissolved in Qiagen RLT Plus lysis buffer
601 supplemented with 1% β-mercaptoethanol and centrifuged for 3 min at maximum speed. The
602 supernatant was transferred to a gDNA Eliminator spin column to remove genomic DNA, and the
603 flow-through was mixed with 70% ethanol and placed in an RNeasy spin column. After one wash
604 with the RW1 buffer and two washes with the RPE buffer, RNA was eluted in 20uL of RNase-free
605 water and quantified using a NanoDrop 1000 Spectrophotometer (ThermoFisher). RNA
606 concentration was normalized to 20ng/uL, and 150ng of total RNA was shipped to NanoString
607 Technologies® (Seattle, WA, USA) for analysis.
608
609

610 **NanoString neuropathology panel gene expression profiling**

611 The NanoString Neuropathology profile panel was used for gene expression profiling of our RNA
612 samples on the nCounter platform (NanoString Technologies®, Seattle, WA, USA). The
613 neuropathology panel incorporated 770 human genes, including 10 references (housekeeping
614 genes) and 760 endogenous genes, to target all aspects of neurodegeneration. Data were
615 analyzed by ROSALIND® (https://rosalind.onramp.bio), with a Hyperscale architecture developed
616 by ROSALIND, Inc. (San Diego, CA, USA). Normalization, fold changes, and p-values were
617 calculated using criteria provided by NanoString. ROSALIND® follows the nCounter® Advanced
618 Analysis protocol of dividing counts within a lane by the geometric mean of the normalizer probes
619 from the same lane.

620 Housekeeping probes for normalization were selected based on the geNorm algorithm
621 implemented in the NormqPCR R library [64]. Fold changes and significance score (p-value) were
622 calculated using the optimal method described in the nCounter® Advanced Analysis 2.0 User
623 Manual. Significant p-values ($p < 0.05$) were adjusted for multiple genetic comparisons using the
624 Benjamini–Hochberg method of estimating false discovery rates [65]. Gene expression was
625 considered significantly different if there was a greater than 1.5. fold change compared to controls.
626 The nCounter Neuropathology profile panel annotation database was referenced to perform gene
627 set enrichment analysis. Directed global significance scores (GSS) were calculated relative to a
628 set of background genes measured in the experiment. This analysis determined both significance
629 and directional response (i.e., upregulated or downregulated) of GSS for a given
630 neurodegeneration pathway. A total of 24 fundamental neurodegeneration pathways were
631 examined to determine the effect of FAD mutation. Bar plots were generated to compare
632 neurodegeneration pathways as a function of directed GSS.

633

634

635

636 **AMP-AD post-mortem brain cohorts and gene co-expression modules**

637 Data on the 30 human AMP-AD co-expression modules were obtained from the Synapse data
638 repository [56, 58, 66] (https://www.synapse.org/#!Synapse:syn11932957/tables/;SynapseID:
639 syn11932957). These modules were obtained from a co-expression meta-analysis of harmonized
640 AMP-AD data across three independent study cohorts. Each module is enriched in genes
641 differentially expressed in AD cases versus controls [17]. The 30 AMP-AD modules were further
642 grouped into five consensus clusters that describe the major functional groups of alterations
643 observed in human AD [17, 51].

644

645 **iPSC-derived cultures-human brains expression comparison**

646 The nSolver software-generated raw gene expression counts for the Neuropathology panel.
647 Normalization was done by dividing counts within a lane by the geometric mean of the
648 housekeeping genes from the same lane. Next, normalized count values were log-transformed
649 for downstream analysis. To determine the effect of FAD mutation, we fitted a linear mixed-effect
650 regression model using the lme4 function in R by considering the fixed effect of FAD mutation
651 plus random variation in intercept among cell lines within controls and FAD mutation (formula ~
652 FAD + 1|FAD:Cell.Line).

653 To compare expression changes in FAD lines with those observed in human disease, we
654 computed Pearson correlations between log fold change in transcript expression of human AD
655 patients compared to control patients (Log2FC(AD/controls) and the effect of FAD mutation
656 estimated by the linear mixed-effect regression model [51, 67]. Correlation coefficients were
657 computed using the cor.test function built-in R as: cor.test(log2FC(AD/Control,β_{FAD}).

658 LogFC values for human transcripts after correction for technical covariates were obtained via the
659 AD Knowledge Portal (https://www.synapse.org/#!Synapse:syn14237651).

660

661

662 **Statistical analysis**

663 Information regarding statistical analyses can be found in the figure legends. Data are expressed
664 as the mean ± standard error of the mean (SEM), represented as error bars. All statistical tests
665 were computed using GraphPad Prism 9 software unless otherwise noted. ROUT method (1%)
666 was applied to identify outliers. A p-value of 0.05 was used as the significance threshold
667 throughout this study. In all figures, p-values are illustrated for all tests used: $^{n.s.}$ $p > 0.05$, * $p <$
668 0.05, ** $p \leq 0.01$, *** $p \leq 0.001$, **** $p \leq 0.0001$. A minimum of two differentiations for each iPSC
669 line have been analyzed for all experiments. Figure legends and graphs representing individual
670 data points indicate the sample size (n = number of scaffolds).

671

672 **List of supplementary materials:** Fig. S1, Fig. S2, Fig. S3, Fig. S4, Antibody Table.

673 **Availability of data and materials:** All data generated or analyzed during this study are included
674 in this published article and its supplementary information files. Additional information is available
675 from the corresponding author on request. ROSMAP resources can be requested at
676 https://www.radc.rush.edu.

677 **Competing interests:** SL, RSP, NR, BM, WK, WLC, PGH, DAB, TLYP, GWC, DLK, and GT have
678 no conflict of interest to declare.

679 **Funding:** This work was supported by awards from the National Institutes of Health:
680 1R21AG065792 (to GT), 5R01AG061838 (to GT, PGH, and DLK), R01AG055909 (to TLYP), and
681 U54AG054345 (to GWC). ROSMAP is supported by P30AG10161, P30AG72975, R01AG15819,
682 R01AG17917. U01AG46152, U01AG61356 (to DAB).

683 **Authors' contributions:** The authors confirm contributions to the manuscript as follows:
684 conceptualization: SL, GT; data curation: SL, RSP, NR; formal analysis: SL, RSP, NR;

investigation: SL, NR, BM, WK, WLC; methodology: SL, RSP, NR, GWC; resources: WLC, GWC, DAB, TLYP, DLK; project administration: GT; supervision: SL, GWC, DLK, GT; validation: SL, RSP, NR, BM, WK, GT; visualization: SL, RSP, NR; writing - original draft preparation: SL, RSP, NR, GT; writing - review and editing: SL, RSP, NR, BM, WK, WLC, PGH, DAB, TLYP, GWC, DLK, GT.

Acknowledgments: We thank Rachel Willen, Edward K. Robinson, Griffin Sigal, and Isabel Paine for their technical support.

Abbreviations:

2D: Two-Dimensional

3D: Three-Dimensional

Aβ: Amyloid Beta

AD: Alzheimer's Disease

AMP-AD: Accelerating Medicines Partnership for Alzheimer's Disease

AP: Action Potential

APP: Amyloid Precursor Protein

CBE: Cerebellum

CSF: Cerebrospinal Fluid

DEG: Differentially Expressed Gene

DIAN: Dominantly Inherited Alzheimer's Network

EB: Embryoid Body

EP: Evoked Potential

FAD: Familial Alzheimer's Disease

GFAP: Glial Fibrillary Acidic Protein

GSA: Gene Set Analysis

710 hNeuron: Human Neuron

711 IFG: Inferior Frontal Gyrus

712 iPSC: Induced Pluripotent Stem Cell

713 LOAD: Late-Onset Alzheimer's Disease

714 LFP: Local Field Potential

715 MAP2B: Microtubule-Associated Protein 2B

716 MSD: Meso Scale Discovery

717 NFH: Neurofilament Heavy Chain

718 NFT: Neurofibrillary Tangles

719 NPC: Neural Precursor Cell

720 Oct4: Octamer-Binding Transcription Factor 4

721 PHG: Parahippocampus Gyrus

722 PSEN1: Presenilin 1

723 PSEN2: Presenilin 2

724 ROSMAP: Religious Order Study Rush Memory and Aging Project

725 SYN: Synaptophysin

726 TCX: Temporal Cortex

727 Tuj1: Neuron-Specific Class III Beta-Tubulin

728

729

730

731

732

733 **Figures**

734 **Figure 1**

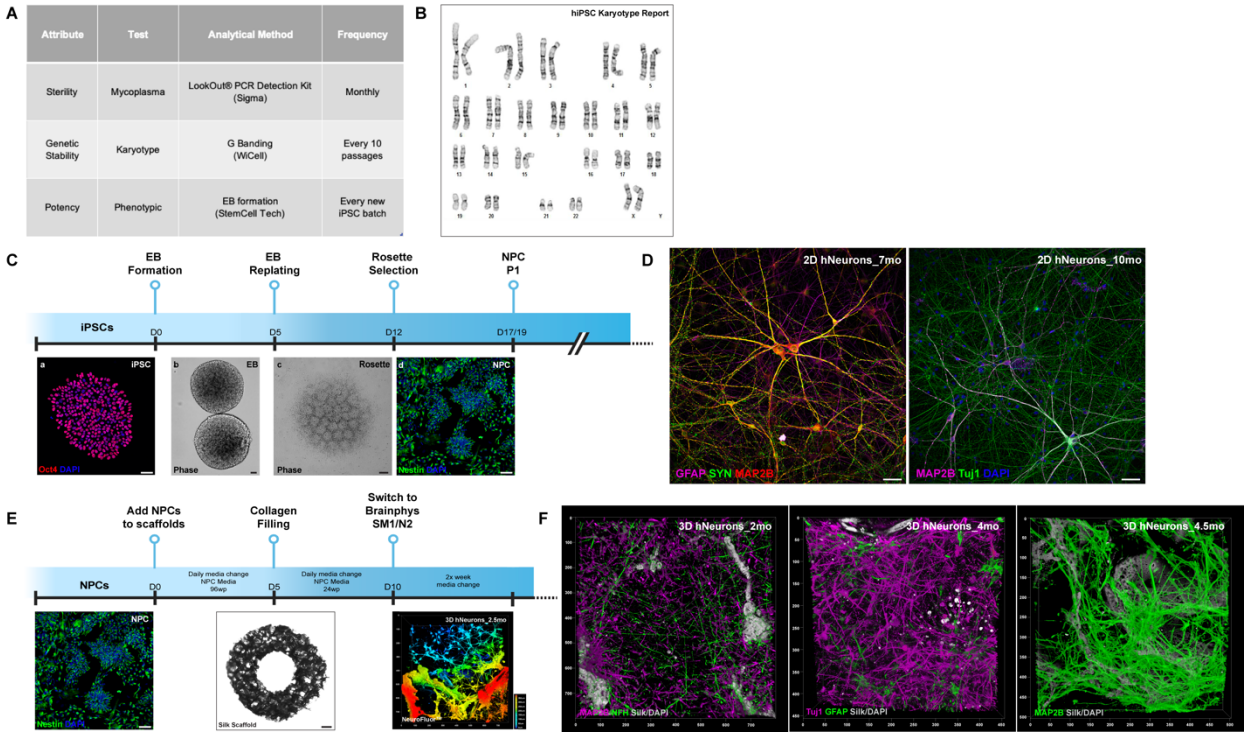

735

736 **Figure 1:** (A) Quality tests performed on iPSCs used in this study. (B) Representative karyotype
737 report. Reports for all the lines are in Fig. S1. (C) Schematic representation of the differentiation
738 timeline to generate NPCs. (a) Representative iPSC colony stained for Oct4 (red) and DAPI
739 (blue). Scale bar: 40um. Confocal z-stack. Leica SP8 HC PL APO CS2 20x/0.75 IMM. 1.5x Zoom.
740 EB (b) and rosettes (c) phase-contrast images. Scale bar: 20um. Nikon TE300 CFI PL FL DL
741 4x/0.13 and 10x/0.30. (d) NPC cultures stained for nestin (green) and DAPI (blue). Scale bar:
742 40um. Confocal z-stack. Leica SP8 HC PL APO CS2 20x/0.75 IMM. 1x Zoom. (D) 2D 7-months-
743 old hNeurons stained for GFAP (magenta), SYN (green), and MAP2B (red), and 10-months-old
744 hNeurons stained for MAP2B (magenta), Tuj1 (green), and DAPI (blue). Scale bar: 50um.
745 Confocal z-stack. Leica SP8 HC PL APO CS2 20x/0.75 IMM. 0.75x Zoom. (E) Schematic
746 representation of the timeline to differentiate hNeurons in silk-collagen scaffolds from NPCs. Silk

747 scaffold phase-contrast image. Scale bar: 500um. Z-stack. Stitched image. Zeiss CD7 PL APO
748 5x/0.35. Magnification changer 0.5x. 3D reconstruction of hNeurons grown in a scaffold for 2.5
749 months and stained with NeuroFluor™ NeuO. Leica SP8 HC PL APO CS2 20x/0.75 IMM. 0.75x
750 Zoom. (F) 3D reconstruction of hNeurons grown in a scaffold for 2 months (stained for MAP2B
751 (magenta), NFH (green)), 4 months (stained for Tuj1 (magenta), GFAP (green)) and 4.5 months
752 (stained for MAP2B (green)). For all the images DAPI and silk autofluorescent signals are in grey.
753 Leica SP8 HC PL APO CS2 20x/0.75 IMM. 0.75x Zoom.

754

755

756

757

758

759

760

761

762

763

764

765

766 **Figure 2**

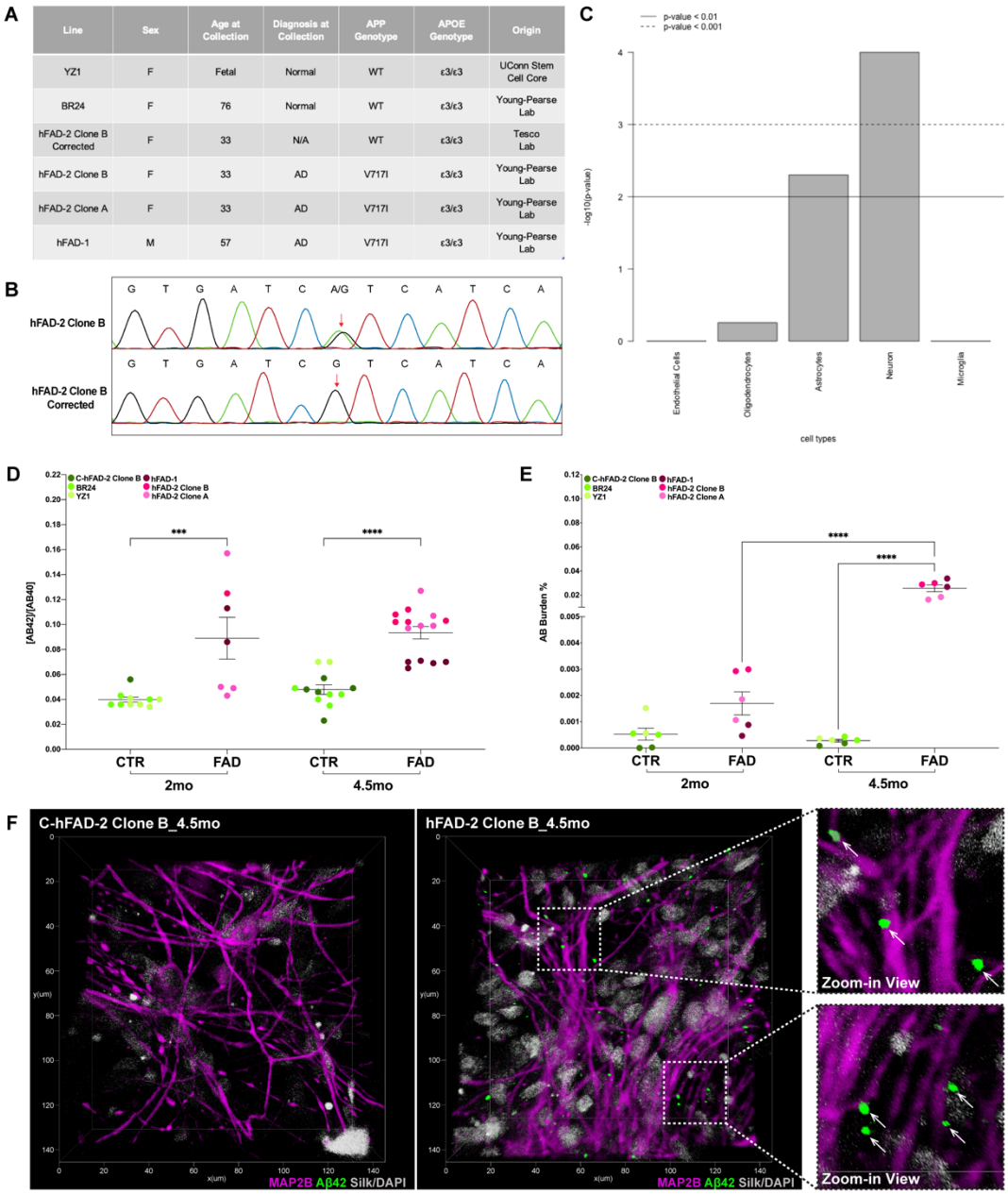

767

768 **Figure 2:** (A) Table reporting iPS lines used across the study. (B) Sequencing traces of hFAD-2

769 Clone B and its isogenic control after reversion of the APP V717I mutation (C-hFAD-2 Clone B).

770 (C) nSolver Cell Enrichment analysis bar plot. (D) Aβ42/40 MSD analysis quantification in

771 conditioned media. FAD cultures (hFAD-1, hFAD-2 Clone A, hFAD-2 Clone B) and controls (C-

772 hFAD-2 Clone B, BR24, YZ1) plotted as groups are provided at 2 and 4.5 months. CTR 2mo:
773 n=10, FAD 2mo: n=7, CTR 4.5mo: n=12, FAD 4.5mo: n=15. One-way ANOVA, Tukey's post-hoc
774 test. (E) Amyloid burden quantification (%). FAD cultures (hFAD-1, hFAD-2 Clone A, hFAD-2
775 Clone B) and controls (C-hFAD-2 Clone B, BR24, YZ1) plotted as groups are provided at 2 and
776 4.5 months. n=6. One-way ANOVA, Tukey's post-hoc test. (E) Representative 3D reconstructions
777 of hNeuron culture (4.5 months) derived from C-hFAD-2 Clone B and hFAD-2 Clone B stained for
778 MAP2B (magenta) and Aβ42 (green). DAPI and silk autofluorescent signals are in grey. Zoom-in
779 view: green Aβ42 extracellular depositions (white arrows) interspersed among hNeurons
780 (MAP2B, magenta). Leica Falcon SP8 HC PL APO CS2 20x/0.75 IMM. 3.5x Zoom.

781 **Figure 3**

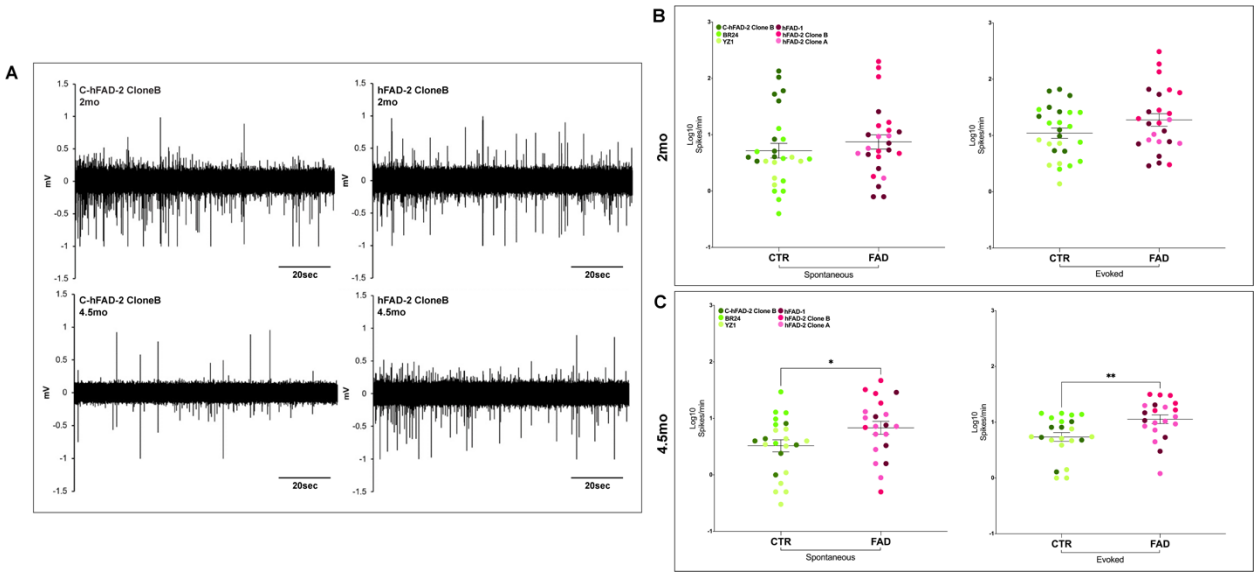

782

783 **Figure 3:** (A) Representative traces of spontaneous LFPs (mV) obtained from 3D cultures derived
784 from a FAD line (hFAD-2 Clone B) and the isogenic control (C-hFAD-2 Clone B) at 2 months and
785 4.5 months. A 20-sec reference is provided for traces. Quantification of normalized spontaneous
786 and evoked LFP spikes/min (Log10) at 2 months (B) and 4.5 months (C). FAD cultures (hFAD-1,
787 hFAD-2 Clone A, hFAD-2 Clone B) and controls (C-hFAD-2 Clone B, BR24, YZ1) plotted as

788 groups are provided. (B) Spontaneous CTR 2mo n=26, FAD 2mo n=25. Evoked CTR 2mo n=26,

789 FAD 2mo n=25. (C) Spontaneous CTR 4.5mo n=23, FAD 4.5mo n=21. Evoked CTR 4.5mo n=22,

790 FAD 4.5mo n=21. Unpaired t-test.

791 **Figure 4**

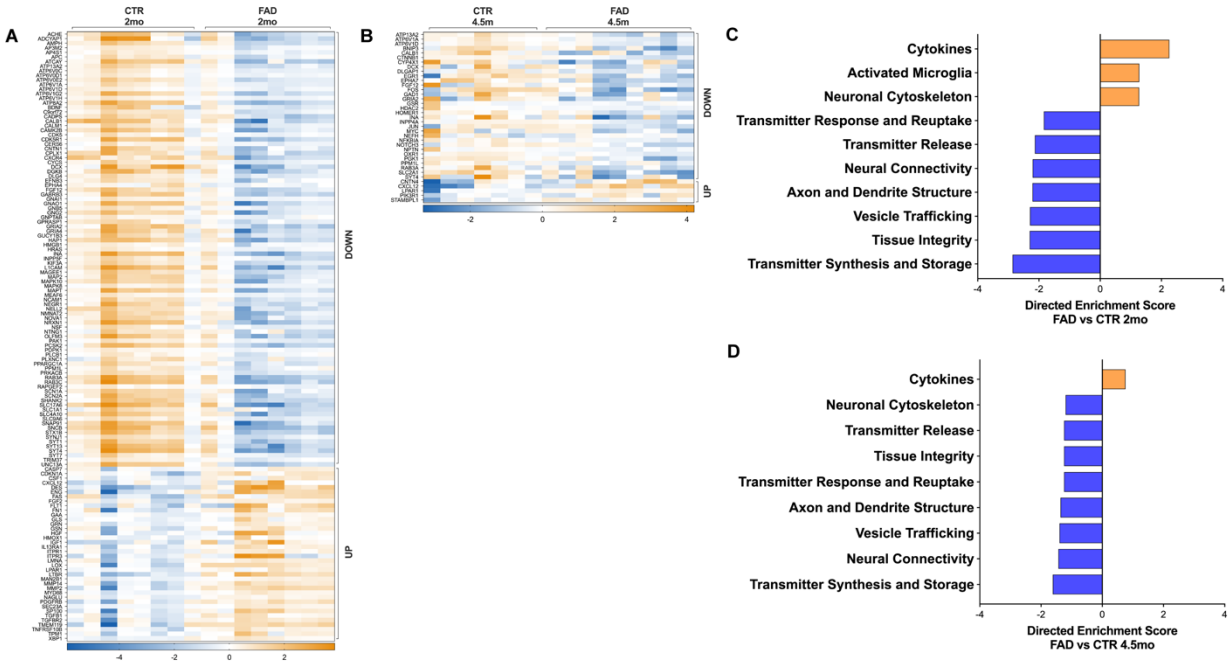

792

793 **Figure 4**: DEGs (absolute fold change > 1.5, FDR < 0.05) in 2-months-old (A) and 4.5-months-

794 old (B) CTR and FAD lines, are shown in the heatmap. GSA of differentially expressed genes in

795 iPSC-derived cultures (FAD vs CTR, ROSALIND® platform, NanoString annotations) at 2 months

796 (C) and 4.5 months (D). Upregulation: directed enrichment score > 0. Downregulation: directed

797 enrichment score < 0. FAD 2mo n=8, CTR 2mo n=8, FAD 4.5mo n=9, CTR 4.5mo n=7.

798

799

800

801 **Figure 5**

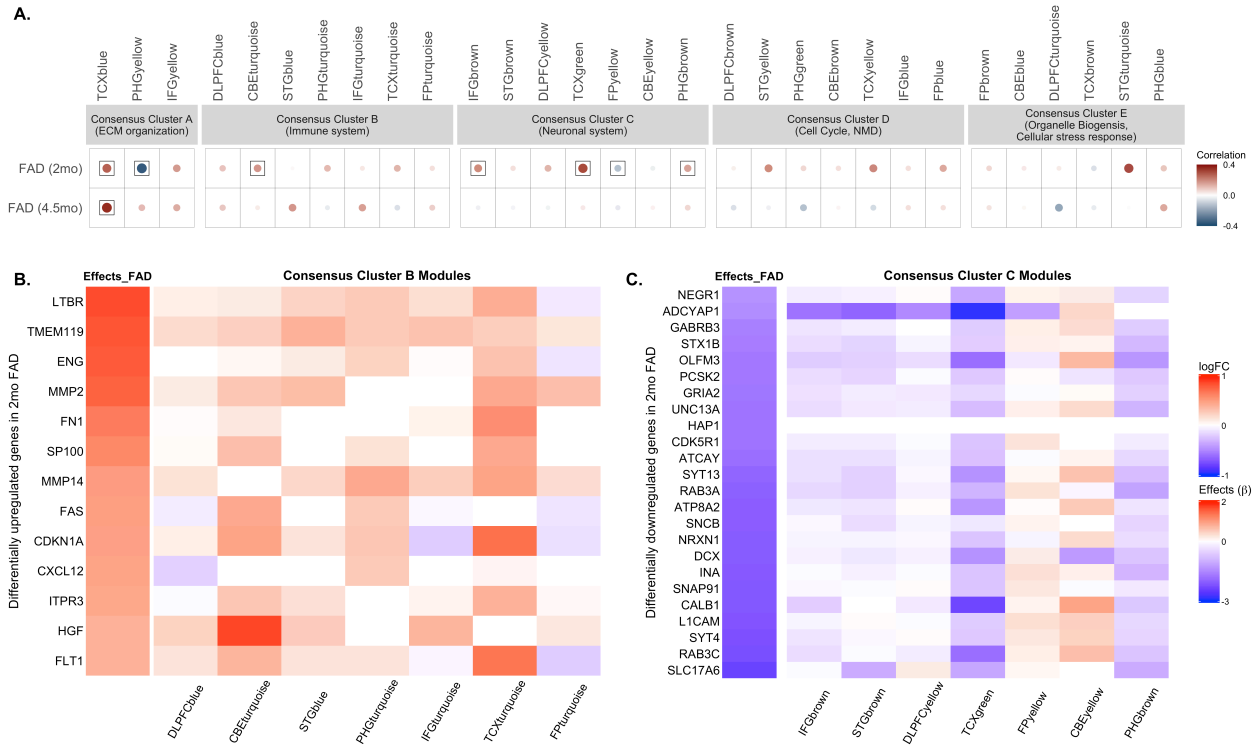

802

803 **Figure 5:** Correlation analysis between the gene expression profile of FAD cultures and human
804 post-mortem co-expression modules. (A) 2-months-old FAD cultures exhibited a significant
805 positive correlation ($p < 0.05$) with AD changes in immune-related modules in Consensus Cluster
806 B and neuronal related modules in Consensus Cluster C. Circles within a square correspond to
807 significant ($p < 0.05$) positive (red) and negative (blue) Pearson correlation coefficients for gene
808 expression changes in FAD lines associated with disease-associated changes in distinct human
809 co-expression modules. Color intensity and size of the circles are proportional to the correlation.
810 (B) Differentially upregulated genes in the 2 months old FAD lines (FDR <0.05, fold change >
811 1.5), showing increased expression in immune/inflammation associated AMP-AD modules in
812 Consensus Cluster B, are shown in the heatmap. (C) Differentially downregulated genes in the 2
813 months old FAD lines (FDR <0.05, fold change < 1.5), exhibiting reduced expression in neuronal-

associated AMP-AD modules in Consensus Cluster C, are shown in the heatmap. FAD 2mo n=8, CTR 2mo n=8.

Figure S1

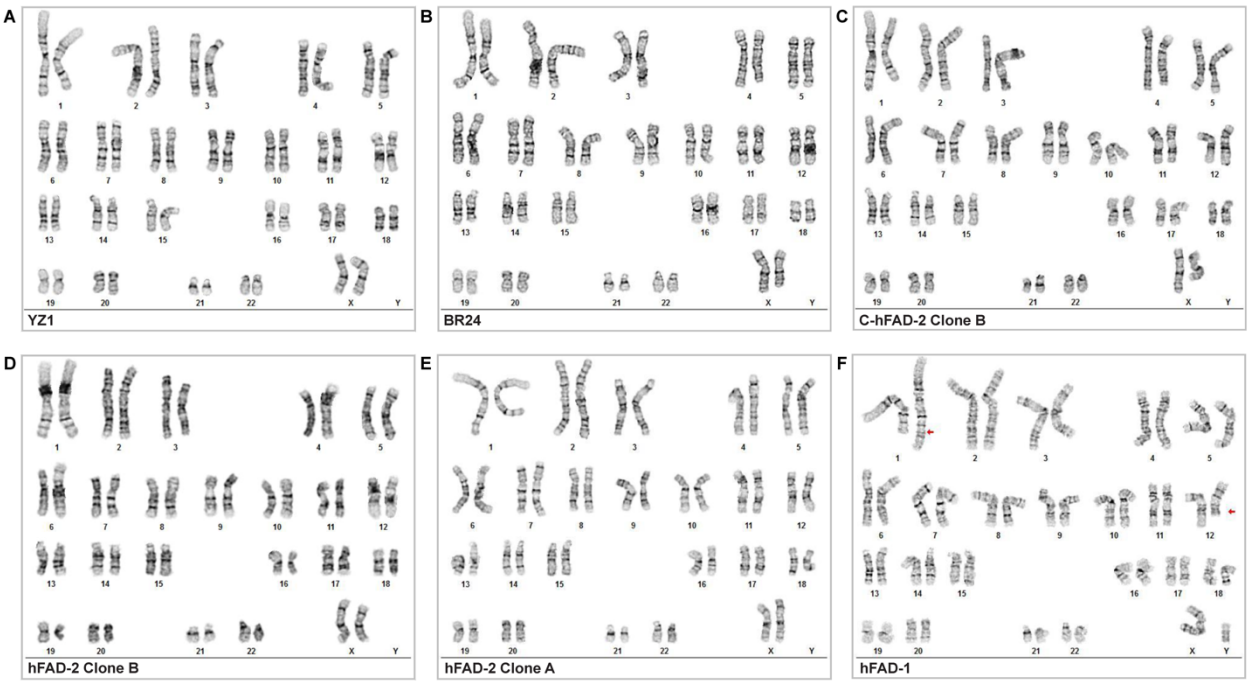

Figure S1: Karyotype reports for all the lines used across the study (WiCell).

825 **Figure S2**

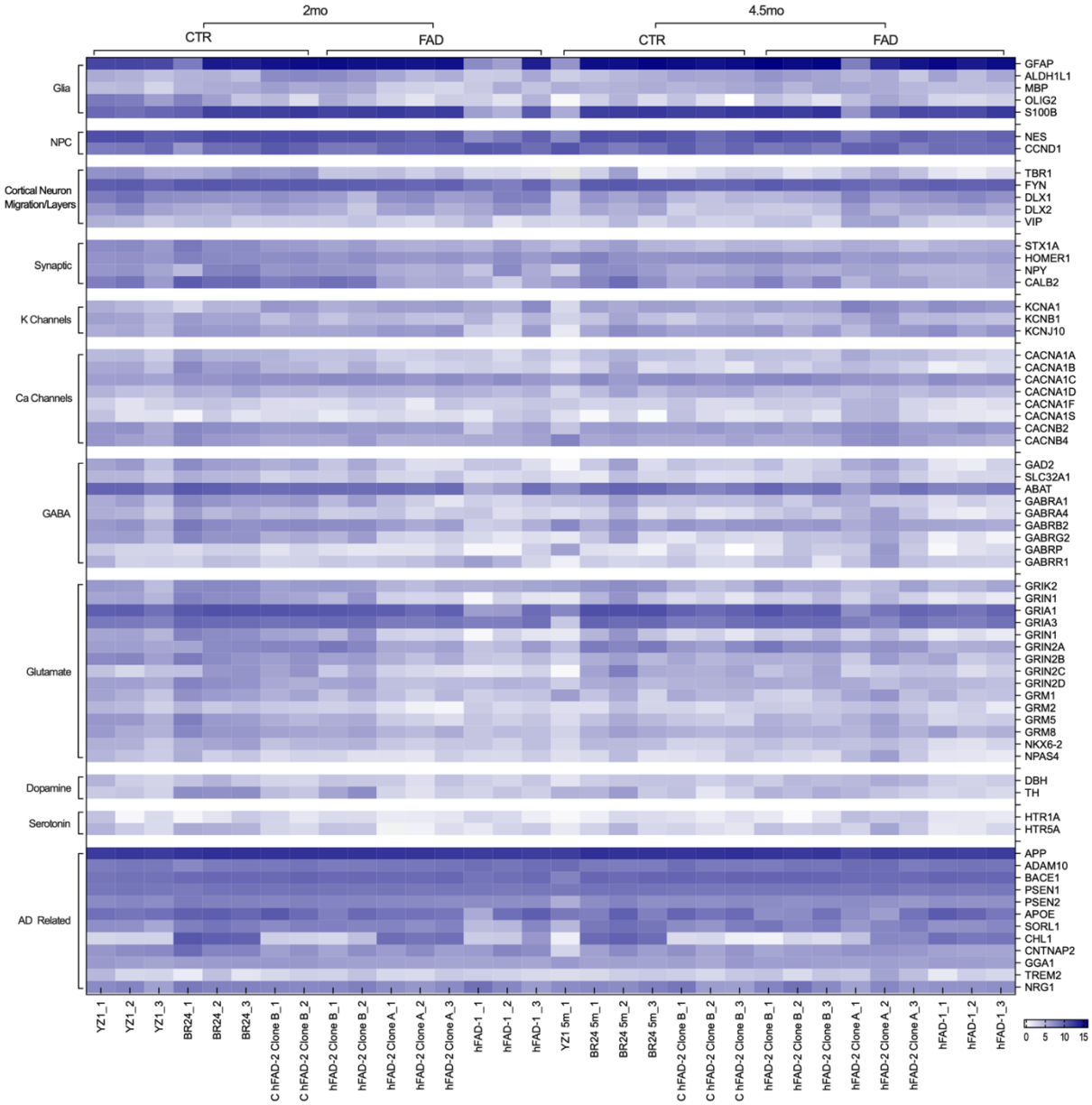

826

827 **Figure S2:** Normalized expression heatmap (9 housekeeping probes) of genes used to
828 characterize the 3D cultures. FAD 2mo n=8, CTR 2mo n=8, FAD 4.5mo n=9, CTR 4.5mo n=7.
829 Genes included in the heatmap are not deregulated when comparing FAD vs. CTR lines at any
830 time point analyzed.

831 **Figure S3**

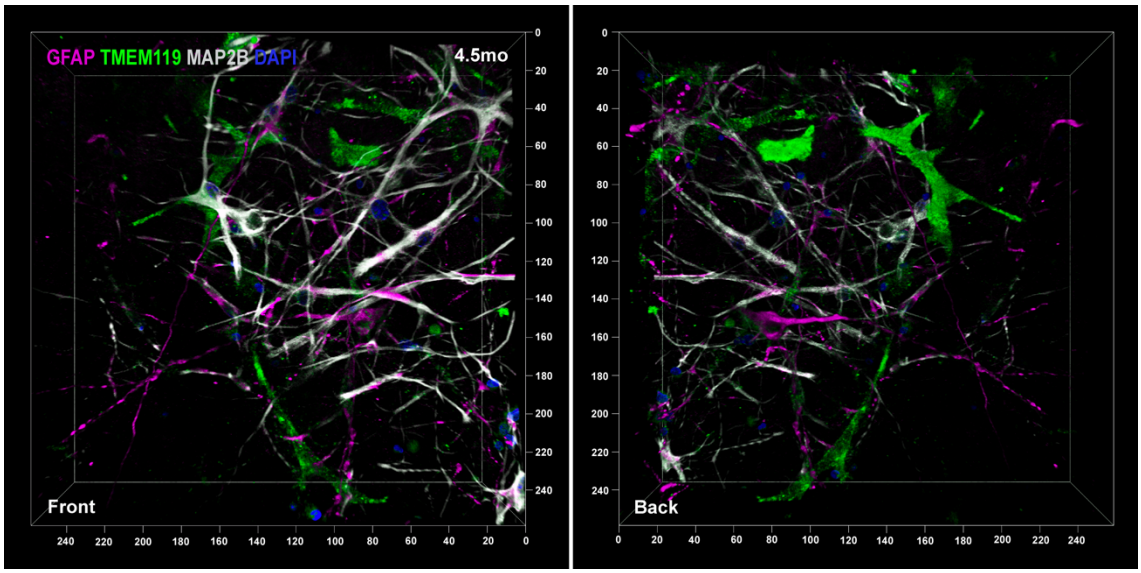

832

833 **Figure S3:** 3D reconstruction of 4.5 months cultures (stained for MAP2B (grey), TMEM119

834 (green), GFAP (magenta), DAPI (blue)). Front and back projections are shown. Leica Falcon SP8

835 HC PL APO CS2 20x/0.75 IMM. 2.25x Zoom.

836 **Figure S4**

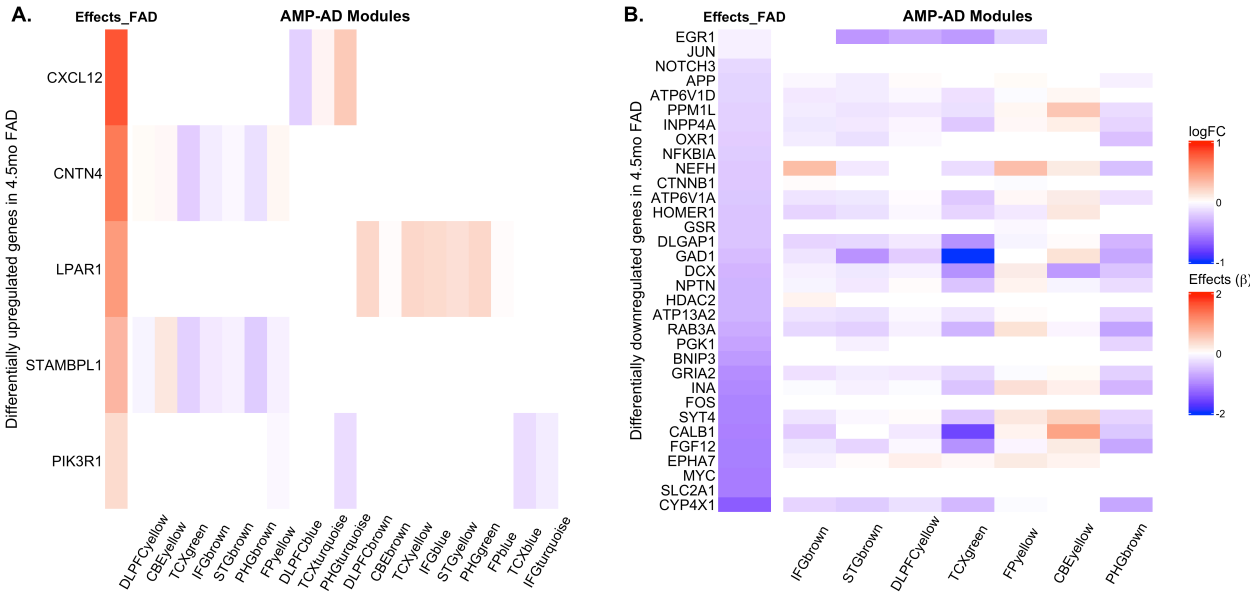

837

838 **Figure S4:** Gene expression changes of differentially expressed genes in the 4.5-months-old
839 FAD cultures across human co-expression modules. (A) Gene expression changes of five
840 differentially upregulated genes in the 4.5-months-old FAD lines (FDR <0.05, fold change > 1.5)
841 across AMP-AD modules are shown in the heatmap. (B) Gene expression changes of
842 differentially downregulated genes in the 4.5-months-old FAD lines (FDR <0.05, fold change <
843 1.5) across AMP-AD. FAD 4.5mo n=9, CTR 4.5mo n=7.

844 **Antibody Table**

Target Antigen	Host	Clone	Clonality	Reactive Species	Company	Catalog #	IF Dilution	
							2D	3D
Aβ42	Rabbit	H31L21	Monoclonal	Human, Mouse	Invitrogen	700254	/	1:200
GFAP	Rabbit	/	Polyclonal	Human 90-95% homology between species	Dako	Z0334	1:1000	1:500
GFAP	Mouse	G-A-5	Monoclonal	Pig, Rat, Human	Sigma	G3893	/	1:500
MAP2B	Mouse	18	Monoclonal	Rat, Human, Mouse	BD Biosciences	610460	1:1000	1:500
MAP2B	Chicken	/	Polyclonal	Human, Rat, Bovine	Millipore	AB5543	1:1000	1:500
Nestin	Mouse	10C2	Monoclonal	Human Non-Human Primate	StemCell Tech	10C2	1:1000	/
NFH	Chicken	/	Polyclonal	Human, Rat, Mouse, Bovine, Porcine, Feline	Millipore	AB5539	/	1:500
OCT4	Mouse	3A2A20	Monoclonal	Human	StemCell Tech	60093	1:250	/
Synaptophysin 1	Mouse	7.2	Monoclonal	Human, Rat, Mouse, Mammals	Synaptic Systems	101011	1:500	/
TMEM119	Rabbit	/	Polyclonal	Human	Sigma	HPA051870	/	1:200
Tuj1	Mouse	TU-20	Monoclonal	Bovine, Rat, Avian, Monkey, Sheep, Human, Mouse, Pig	Chemicon	MAB1637	1:1000	1:500

845

846

847
848
849
850
851
852
853
854

855 **Bibliography**
856

857 1. Serrano-Pozo A, Frosch MP, Masliah E, Hyman BT: **Neuropathological alterations in**
858 **Alzheimer disease.** *Cold Spring Harb Perspect Med* 2011, **1:**a006189.

859 2. Qiu C, Kivipelto M, von Strauss E: **Epidemiology of Alzheimer's disease: occurrence,**
860 **determinants, and strategies toward intervention.** *Dialogues Clin Neurosci* 2009, **11:**111-
861 128.

862 3. D'Avanzo C, Aronson J, Kim YH, Choi SH, Tanzi RE, Kim DY: **Alzheimer's in 3D culture:**
863 **challenges and perspectives.** *Bioessays* 2015, **37:**1139-1148.

864 4. Miller JA, Horvath S, Geschwind DH: **Divergence of human and mouse brain**
865 **transcriptome highlights Alzheimer disease pathways.** *Proc Natl Acad Sci U S A* 2010,
866 **107:**12698-12703.

867 5. Zhang Y, Sloan SA, Clarke LE, Caneda C, Plaza CA, Blumenthal PD, Vogel H, Steinberg GK,
868 Edwards MS, Li G, et al: **Purification and Characterization of Progenitor and Mature**
869 **Human Astrocytes Reveals Transcriptional and Functional Differences with Mouse.**
870 *Neuron* 2016, **89:**37-53.

871 6. Arranz AM, De Strooper B: **The role of astroglia in Alzheimer's disease: pathophysiology**
872 **and clinical implications.** *Lancet Neurol* 2019, **18:**406-414.

873 7. Penney J, Ralvenius WT, Tsai LH: **Modeling Alzheimer's disease with iPSC-derived brain**
874 **cells.** *Mol Psychiatry* 2020, **25:**148-167.

875 8. Cenini G, Hebisch M, Iefremova V, Flitsch LJ, Breitkreuz Y, Tanzi RE, Kim DY, Peitz M,
876 Brustle O: **Dissecting Alzheimer's disease pathogenesis in human 2D and 3D models.**
877 *Mol Cell Neurosci* 2021, **110:**103568.

878 9. Lagomarsino VN, Pearse RV, Liu L, Hsieh Y-C, Fernandez MA, Vinton EA, Paull D, Felsky D,
879 Tasaki S, Gaiteri C, et al: **Stem cell-derived neurons reflect features of protein networks,**
880 **neuropathology, and cognitive outcome of their aged human donors.** *Neuron* 2021,
881 **109:**3402-3420.e3409.

882 10. Cantley W, Du C, Lomoio S, DePalma T, Peirent E, Kleinknecht D, Hunter M, Tang-Schomer
883 M, Tesco G, Kaplan D: **Functional and Sustainable 3D Human Neural Network Models**
884 **from Pluripotent Stem Cells.** *ACS Biomater Sci Eng,* 2018, **Article ASAP DOI:**
885 **10.1021/acsbiomaterials.8b00622 Publication Date (Web): October 1, 2018**.

886 11. Tang-Schomer MD, White JD, Tien LW, Schmitt LI, Valentin TM, Graziano DJ, Hopkins AM,
887 Omenetto FG, Haydon PG, Kaplan DL: **Bioengineered functional brain-like cortical tissue.**
888 *Proceedings of the National Academy of Sciences of the United States of America* 2014,
889 **111:**13811-13816.

890 12. Cairns DM, Rouleau N, Parker RN, Walsh KG, Gehrke L, Kaplan DL: **A 3D human brain-like**
891 **tissue model of herpes-induced Alzheimer's disease.** *Sci Adv* 2020, **6:**eaay8828.

892 13. Cairns DM, Chwalek K, Moore YE, Kelley MR, Abbott RD, Moss S, Kaplan DL: **Expandable**
893 **and rapidly differentiating human induced neural stem cell lines for multiple tissue**
894 **engineering applications.** *Stem cell reports* 2016, **7:**557-570.

895 14. Rouleau N, Cantley WL, Liaudanskaya V, Berk A, Du C, Rusk W, Peirent E, Koester C,
896 Nieland TJF, Kaplan DL: **A Long-Living Bioengineered Neural Tissue Platform to Study**
897 **Neurodegeneration.** *Macromolecular Bioscience* 2020, **20:**e2000004.

898 15. Muratore CR, Rice HC, Srikanth P, Callahan DG, Shin T, Benjamin LN, Walsh DM, Selkoe
899 DJ, Young-Pearse TL: **The familial Alzheimer's disease APPV717I mutation alters APP**
900 **processing and Tau expression in iPSC-derived neurons.** *Hum Mol Genet* 2014, **23:**3523-
901 3536.

902 16. Hector A, Brouillette J: **Hyperactivity Induced by Soluble Amyloid-beta Oligomers in the**
903 **Early Stages of Alzheimer's Disease.** *Front Mol Neurosci* 2020, **13:**600084.

904 17. Wan YW, Al-Ouran R, Mangleburg CG, Perumal TM, Lee TV, Allison K, Swarup V, Funk CC,
905 Gaiteri C, Allen M, et al: **Meta-Analysis of the Alzheimer's Disease Human Brain**
906 **Transcriptome and Functional Dissection in Mouse Models.** *Cell Rep* 2020, **32:**107908.

907 18. Chwalek K, Tang-Schomer MD, Omenetto FG, Kaplan DL: **In vitro bioengineered model of**
908 **cortical brain tissue.** *Nature Protocols* 2015, **10:**1362-1373.

909 19. Nazarov R, Jin HJ, Kaplan DL: **Porous 3-D scaffolds from regenerated silk fibroin.**
910 *Biomacromolecules* 2004, **5:**718-726.

911 20. Muratore CR, Srikanth P, Callahan DG, Young-Pearse TL: **Comparison and optimization**
912 **of hiPSC forebrain cortical differentiation protocols.** *Plos One* 2014, **9:**e105807.

913 21. Itskovitz-Eldor J, Schuldiner M, Karsenti D, Eden A, Yanuka O, Amit M, Soreq H, Benvenisty
914 N: **Differentiation of human embryonic stem cells into embryoid bodies compromising**
915 **the three embryonic germ layers.** *Molecular Medicine* 2000, **6:**88-95.

916 22. Zeng H, Guo M, Martins-Taylor K, Wang X, Zhang Z, Park JW, Zhan S, Kronenberg MS,
917 Lichtler A, Liu H-X, et al: **Specification of region-specific neurons including forebrain**
918 **glutamatergic neurons from human induced pluripotent stem cells.** *Plos One* 2010,
919 **5:**e11853.

920 23. Muratore CR, Zhou C, Liao M, Fernandez MA, Taylor WM, Lagomarsino VN, Pearse RV, Rice
921 HC, Negri JM, He A, et al: **Cell-type Dependent Alzheimer's Disease Phenotypes: Probing**
922 **the Biology of Selective Neuronal Vulnerability.** *Stem cell reports* 2017, **9:**1868-1884.

923 24. Engle SJ, Blaha L, Kleiman RJ: **Best Practices for Translational Disease Modeling Using**
924 **Human iPSC-Derived Neurons.** *Neuron* 2018, **100:**783-797.

925 25. Pettinato G, Wen X, Zhang N: **Formation of well-defined embryoid bodies from**
926 **dissociated human induced pluripotent stem cells using microfabricated cell-repellent**
927 **microwell arrays.** *Sci Rep* 2014, **4:**7402.

928 26. Topol A, Tran NN, Brennand KJ: **A guide to generating and using hiPSC derived NPCs**
929 **for the study of neurological diseases.** *J Vis Exp* 2015**:**e52495.

930 27. Readhead B, Hartley BJ, Eastwood BJ, Collier DA, Evans D, Farias R, He C, Hoffman G,
931 Sklar P, Dudley JT, et al: **Expression-based drug screening of neural progenitor cells**
932 **from individuals with schizophrenia.** *Nat Commun* 2018, **9:**4412.

933 28. Bennett DA, Buchman AS, Boyle PA, Barnes LL, Wilson RS, Schneider JA: **Religious Orders**
934 **Study and Rush Memory and Aging Project.** *J Alzheimers Dis* 2018, **64:**S161-S189.

935 29. Danaher P, Warren S, Dennis L, D'Amico L, White A, Disis ML, Geller MA, Odunsi K,
936 Beechem J, Fling SP: **Gene expression markers of Tumor Infiltrating Leukocytes.** *J*
937 *Immunother Cancer* 2017, **5:**18.

938 30. Zhang Y, Pak C, Han Y, Ahlenius H, Zhang Z, Chanda S, Marro S, Patzke C, Acuna C, Covy
939 J, et al: **Rapid single-step induction of functional neurons from human pluripotent stem**
940 **cells.** *Neuron* 2013, **78:**785-798.

941 31. Nehme R, Zuccaro E, Ghosh SD, Li C, Sherwood JL, Pietilainen O, Barrett LE, Limone F,
942 Worringer KA, Kommineni S, et al: **Combining NGN2 Programming with Developmental**
943 **Patterning Generates Human Excitatory Neurons with NMDAR-Mediated Synaptic**
944 **Transmission.** *Cell reports* 2018, **23:**2509-2523.

945 32. Liao M-C, Muratore CR, Gierahn TM, Sullivan SE, Srikanth P, De Jager PL, Love JC, Young-
946 Pearse TL: **Single-Cell Detection of Secreted Aβ and sAPPα from Human IPSC-Derived**
947 **Neurons and Astrocytes.** *The Journal of Neuroscience* 2016, **36:**1730-1746.

948 33. Mariani J, Simonini MV, Palejev D, Tomasini L, Coppola G, Szekely AM, Horvath TL,
949 Vaccarino FM: **Modeling human cortical development in vitro using induced pluripotent**
950 **stem cells.** *Proc Natl Acad Sci U S A* 2012, **109:**12770-12775.

951 34. Arber C, Toombs J, Lovejoy C, Ryan NS, Paterson RW, Willumsen N, Gkanatsiou E, Portelius
952 E, Blennow K, Heslegrave A, et al: **Familial Alzheimer's disease patient-derived neurons**
953 **reveal distinct mutation-specific effects on amyloid beta.** *Mol Psychiatry* 2020, **25:**2919-
954 2931.

955 35. O'Connor A, Pannee J, Poole T, Arber C, Portelius E, Swift IJ, Heslegrave AJ, Abel E,
956 Willumsen N, Rice H, et al: **Plasma amyloid-beta ratios in autosomal dominant**
957 **Alzheimer's disease: the influence of genotype.** *Brain* 2021, **144:**2964-2970.

958 36. Eimer WA, Vassar R: **Neuron loss in the 5XFAD mouse model of Alzheimer's disease**
959 **correlates with intraneuronal Abeta42 accumulation and Caspase-3 activation.** *Mol*
960 *Neurodegener* 2013, **8:**2.

961 37. Du C, Collins W, Cantley W, Sood D, Kaplan DL: **Tutorials for Electrophysiological**
962 **Recordings in Neuronal Tissue Engineering.** *ACS Biomater Sci Eng* 2017, **3:**2235-2246.

963 38. Lam AD, Deck G, Goldman A, Eskandar EN, Noebels J, Cole AJ: **Silent hippocampal**
964 **seizures and spikes identified by foramen ovale electrodes in Alzheimer's disease.** *Nat*
965 *Med* 2017, **23:**678-680.

966 39. Vossel KA, Beagle AJ, Rabinovici GD, Shu H, Lee SE, Naasan G, Hegde M, Cornes SB,
967 Henry ML, Nelson AB, et al: **Seizures and epileptiform activity in the early stages of**
968 **Alzheimer disease.** *JAMA neurology* 2013, **70:**1158-1166.

969 40. Zott B, Busche MA, Sperling RA, Konnerth A: **What Happens with the Circuit in Alzheimer's**
970 **Disease in Mice and Humans?** *Annu Rev Neurosci* 2018, **41:**277-297.

971 41. Zott B, Simon MM, Hong W, Unger F, Chen-Engerer HJ, Frosch MP, Sakmann B, Walsh DM,
972 Konnerth A: **A vicious cycle of beta amyloid-dependent neuronal hyperactivation.**
973 *Science* 2019, **365:**559-565.

974 42. Palop JJ, Chin J, Roberson ED, Wang J, Thwin MT, Bien-Ly N, Yoo J, Ho KO, Yu G-Q,
975 Kreitzer A, et al: **Aberrant excitatory neuronal activity and compensatory remodeling of**
976 **inhibitory hippocampal circuits in mouse models of Alzheimer's disease.** *Neuron* 2007,
977 **55:**697-711.

978 43. Palop JJ, Mucke L: **Network abnormalities and interneuron dysfunction in Alzheimer**
979 **disease.** *Nature Reviews Neuroscience* 2016, **17:**777-792.

980 44. Palop JJ, Mucke L: **Amyloid-beta-induced neuronal dysfunction in Alzheimer's disease:**
981 **from synapses toward neural networks.** *Nature Neuroscience* 2010, **13:**812-818.

982 45. Palop JJ, Mucke L: **Epilepsy and cognitive impairments in Alzheimer disease.** *Arch*
983 *Neurol* 2009, **66:**435-440.

984 46. Busche MA, Chen X, Henning HA, Reichwald J, Staufenbiel M, Sakmann B, Konnerth A:
985 **Critical role of soluble amyloid-beta for early hippocampal hyperactivity in a mouse**
986 **model of Alzheimer's disease.** *Proc Natl Acad Sci U S A* 2012, **109:**8740-8745.

987 47. Busche MA, Eichhoff G, Adelsberger H, Abramowski D, Wiederhold K-H, Haass C,
988 Staufenbiel M, Konnerth A, Garaschuk O: **Clusters of hyperactive neurons near amyloid**
989 **plaques in a mouse model of Alzheimer's disease.** *Science* 2008, **321:**1686-1689.

990 48. Busche MA, Grienberger C, Keskin AD, Song B, Neumann U, Staufenbiel M, Forstl H,
991 Konnerth A: **Decreased amyloid-beta and increased neuronal hyperactivity by**
992 **immunotherapy in Alzheimer's models.** *Nat Neurosci* 2015, **18:**1725-1727.

993 49. Ormel PR, Vieira de Sa R, van Bodegraven EJ, Karst H, Harschnitz O, Sneeboer MAM,
994 Johansen LE, van Dijk RE, Scheefhals N, Berdenis van Berlekom A, et al: **Microglia innately**
995 **develop within cerebral organoids.** *Nat Commun* 2018, **9:**4167.

996 50. Quadrato G, Nguyen T, Macosko EZ, Sherwood JL, Min Yang S, Berger DR, Maria N,
997 Scholvin J, Goldman M, Kinney JP, et al: **Cell diversity and network dynamics in**
998 **photosensitive human brain organoids.** *Nature* 2017, **545:**48-53.

999 51. Preuss C, Pandey R, Piazza E, Fine A, Uyar A, Perumal T, Garceau D, Kotredes KP, Williams
1000 H, Mangravite LM, et al: **A novel systems biology approach to evaluate mouse models**
1001 **of late-onset Alzheimer's disease.** *Mol Neurodegener* 2020, **15:**67.

1002 52. Bateman RJ, Xiong C, Benzinger TL, Fagan AM, Goate A, Fox NC, Marcus DS, Cairns NJ,
1003 Xie X, Blazey TM, et al: **Clinical and biomarker changes in dominantly inherited**
1004 **Alzheimer's disease.** *N Engl J Med* 2012, **367:**795-804.

1005 53. Mondadori CR, Buchmann A, Mustovic H, Schmidt CF, Boesiger P, Nitsch RM, Hock C,
1006 Streffer J, Henke K: **Enhanced brain activity may precede the diagnosis of Alzheimer's**
1007 **disease by 30 years.** *Brain* 2006, **129:**2908-2922.

1008 54. Reiman EM, Quiroz YT, Fleisher AS, Chen K, Velez-Pardo C, Jimenez-Del-Rio M, Fagan AM,
1009 Shah AR, Alvarez S, Arbelaez A, et al: **Brain imaging and fluid biomarker analysis in**
1010 **young adults at genetic risk for autosomal dominant Alzheimer's disease in the**
1011 **presenilin 1 E280A kindred: a case-control study.** *Lancet Neurol* 2012, **11:**1048-1056.

1012 55. Ghatak S, Dolatabadi N, Trudler D, Zhang X, Wu Y, Mohata M, Ambasudhan R, Talantova M,
1013 Lipton SA: **Mechanisms of hyperexcitability in Alzheimer's disease hiPSC-derived**
1014 **neurons and cerebral organoids vs isogenic controls.** *Elife* 2019, **8**.

1015 56. Allen M, Carrasquillo MM, Funk C, Heavner BD, Zou F, Younkin CS, Burgess JD, Chai HS,
1016 Crook J, Eddy JA, et al: **Human whole genome genotype and transcriptome data for**
1017 **Alzheimer's and other neurodegenerative diseases.** *Sci Data* 2016, **3:**160089.

1018 57. De Jager PL, Ma Y, McCabe C, Xu J, Vardarajan BN, Felsky D, Klein HU, White CC, Peters
1019 MA, Lodgson B, et al: **A multi-omic atlas of the human frontal cortex for aging and**
1020 **Alzheimer's disease research.** *Sci Data* 2018, **5:**180142.

1021 58. Wang M, Beckmann ND, Roussos P, Wang E, Zhou X, Wang Q, Ming C, Neff R, Ma W,
1022 Fullard JF, et al: **The Mount Sinai cohort of large-scale genomic, transcriptomic and**
1023 **proteomic data in Alzheimer's disease.** *Sci Data* 2018, **5:**180185.

1024 59. Mertens J, Reid D, Lau S, Kim Y, Gage FH: **Aging in a Dish: iPSC-Derived and Directly**
1025 **Induced Neurons for Studying Brain Aging and Age-Related Neurodegenerative**
1026 **Diseases.** *Annu Rev Genet* 2018, **52:**271-293.

1027 60. Golde TE: **Alzheimer's disease - the journey of a healthy brain into organ failure.** *Mol*
1028 *Neurodegener* 2022, **17:**18.

1029 61. Hronik-Tupaj M, Raja WK, Tang-Schomer M, Omenetto FG, Kaplan DL: **Neural responses**
1030 **to electrical stimulation on patterned silk films.** *J Biomed Mater Res A* 2013, **101:**2559-
1031 2572.

1032 62. Tang-Schomer MD, Hu X, Tupaj M, Tien LW, Whalen M, Omenetto F, Kaplan DL: **Film-based**
1033 **Implants for Supporting Neuron-Electrode Integrated Interfaces for The Brain.** *Adv*
1034 *Funct Mater* 2014, **24:**1938-1948.

1035 63. Rockwood DN, Preda RC, Yucel T, Wang X, Lovett ML, Kaplan DL: **Materials fabrication**
1036 **from Bombyx mori silk fibroin.** *Nat Protoc* 2011, **6:**1612-1631.

1037 64. Perkins JR, Dawes JM, McMahon SB, Bennett DL, Orengo C, Kohl M: **ReadqPCR and**
1038 **NormqPCR: R packages for the reading, quality checking and normalisation of RT-**
1039 **qPCR quantification cycle (Cq) data.** *BMC Genomics* 2012, **13:**296.

1040 65. Ferreira JA: **The Benjamini-Hochberg method in the case of discrete test statistics.** *Int J*
1041 *Biostat* 2007, **3:**Article 11.

1042 66. Mostafavi S, Gaiteri C, Sullivan SE, White CC, Tasaki S, Xu J, Taga M, Klein HU, Patrick E,
1043 Komashko V, et al: **A molecular network of the aging human brain provides insights into**
1044 **the pathology and cognitive decline of Alzheimer's disease.** *Nat Neurosci* 2018, **21:**811-
1045 819.

1046 67. Pandey RS, Graham L, Uyar A, Preuss C, Howell GR, Carter GW: **Genetic perturbations of**
1047 **disease risk genes in mice capture transcriptomic signatures of late-onset Alzheimer's**
1048 **disease.** *Mol Neurodegener* 2019, **14:**50.
1049